MOSPHERIC AND OCEANOGRAPHIC SCIENCES LIBRARY

UME 20

Air-Sea Exchange: Physics, Chemistry and Dynamics

Edited by

G.L. GEERNAERT

National Environmental Research Institute, Roskilde, Denmark

1999, p. 73-126

KLUWER ACADEMIC PUBLISHERS
DORDRECHT / BOSTON / LONDON

Chapter 4

DYNAMICAL COUPLING OF SURFACE WAVES WITH THE ATMOSPHERE

V.K. MAKIN
Royal Netherlands Meteorological Institute (KNMI)
De Bilt, The Netherlands

V.N. KUDRYAVTSEV
Marine Hydrophysical Institute
Sevastopol, Ukraine

4.1 Introduction

The surface transfer processes of momentum, sensible heat, and humidity are strongly affected by the movement and distortion of the ocean surface by the wind, i.e. by wind waves, because these wave motions enhance transfer rates even when the surface is fairly smooth and continuous, and further enhance them when it breaks and forms sea spray. Thus, wind waves being the visual manifestation of the air-sea interaction, play an active role in this process. In fact, wind waves are responsible for the formation and regulation of the surface transfer processes of momentum, sensible heat, and humidity. The reliable estimates of these transfers is of primarily importance for weather prediction and climate studies, forecasting of waves and surge, and for many other meteorological and oceanological applications.

The bulk parameterization relates the fluxes to the local wind speed. Since waves grow, evolve and decay on their own dynamical time/length scales, the fluxes in general cannot be described by the local wind speed alone. In coastal regions, across atmospheric synoptic frontal zones, in the mixed wind wave-swell seas, the sea state varies rapidly in space and time. Here one may expect the momentum flux to depend both on the wind speed and the sea state. Therefore a theory that takes into account the sea state to calculate the momentum flux is required. We call such a theory the wind over waves coupling.

The approach is based on conservation of momentum in the marine atmospheric surface layer, which implies that the total stress above waves, supported both by turbulent motions of the air and by the organised wave-induced motions due to the presence of waves, is independent of height, so that the momentum flux at a given height is equal to the momentum flux at the sea surface. Relating the wave-induced stress (the form drag, that is the correlation of the surface wave-induced pressure with the wave slope) at the surface to the geometrical properties of the surface, described statistically in terms of a wave variance spectrum, and to the properties of the momentum exchange at the surface, the sea drag is thus related (or coupled) directly to waves or the sea state.

A theory of wind over waves coupling was first introduced by Janssen (1989). Applying Miles (1957) theory of the wave growth for a wave spectrum, he found the sea roughness to depend on the coupling parameter (a ratio of the form drag to the total stress) and a background (or local) roughness. The latter is associated by him with the very short gravity waves and irregularities of the surface such as foam, current instabilities and etc., and is parameterized in terms of a Charnock type relation, i.e. proportional to the square of the friction velocity u_* and the acceleration due to gravity g (Charnock 1955). The fact that the background roughness is parameterized with the Charnock relation suggests that gravity waves play an important role. This is at odds with the fact that the contribution of the gravity waves was already accounted for in calculating the wave-induced stress at the surface from the continuous wave spectrum.

Chalikov and Makin (1991), and further Chalikov and Belevich (1993) used the detailed calculations of the turbulent boundary layer above waves of finite amplitude (Makin 1989) to parameterize the vertical distribution of the wave-induced flux. The sea roughness (defined as the constant in the logarithmic wind profile obtained sufficiently far above waves) follows then from a solution of the 1D model of the boundary layer. It is declared that the form of the short gravity wave spectrum is not accurately known, and the form drag is calculated until the cutoff frequency. The form drag associated with shorter waves are parameterized in terms of background roughness. It is assumed that the background roughness is proportional to the height of the short gravity waves. Using the -5 frequency universal Phillips spectrum (Phillips 1966) the background roughness can be related to the Phillips parameter. The height of the short gravity waves scales with u_*^2/g. So, in fact, the Charnock type relation is too used to parameterize the background roughness. The declaration that the short wave spectrum is not known is violated either, as the Phillips spectrum is used to calculate the background roughness. As these short waves are strongly coupled to the atmosphere and support a significant part of the total stress at the surface, parametrization of them in terms of the background roughness parameter makes this wind over waves theory inconsistent.

For seas which are close to fully developed, the use of the Charnock type relations ensures the proper values of the drag coefficients calculated from the models of Janssen (1989) and Chalikov and Makin (1991).

Alternative approaches have been proposed to fix this inconsistency. Caudal (1993) and Jenkins (1993) bypassed this problem by assuming that the total surface stress is supported only by waves, i.e. by the form drag along. This assumption does not hold in general (Makin et al. 1995).

A consistent theory to calculate the sea drag which accounts for the balance between the wave-induced and the turbulent stress at the surface and which avoids the use of the Charnock type relation for the background roughness was introduced by Makin et al. (1995). They assume that the instantaneous sea surface can be treated as a smooth one. That assumption allows them to relate the local roughness length to the scale of the molecular sublayer. Once this assumption has been made the sea roughness can be derived as a result of the balance between the wave-induced and the turbulent stress. The sea roughness, obtained from the model, turns out to be proportional to the friction velocity squared, in close agreement with the Charnock relation.

The bottle neck of all these models is that the momentum flux to waves is very sensible to the form of the high wavenumber part of a wave spectrum, which has to be specified or parameterized in order to calculate the form drag. As was already mentioned, the parameterization of the short waves via the background parameter actually avoids the direct description of coupling and makes a wind over waves theory not consistent.

Though not much is known about the form of the short wave spectrum and its interaction with larger scale oceanic and atmospheric phenomena, it seems more logical to try to describe directly interaction of wind with these waves, if one wants to build a consistent wind over waves coupling theory. Besides, with rapid development of new measurement technics, both contact and remote, the knowledge of short wave spectrum will rapidly grow (Banner et al. 1989; Klinke, Jähne 1992; Hara et al. 1997; Hwang 1996; Hwang et al. 1996).

A reliable statistical description of the short wave spectrum is of crucial importance to better determine the exchange of momentum and heat between the ocean and the atmosphere, as the short gravity and capillary-gravity waves support a significant fraction of the total stress at the sea surface (Makin 1997; Makin, Kudryavtsev 1997).

In the case of remote sensing, short gravity and capillary-gravity waves serve as roughness elements on the ocean surface to scatter electromagnetic waves. Applications of radar instruments for ocean remote sensing then also brought the demand for wave number spectrum models in the short gravity and capillary-gravity range, dynamically coupled with the atmosphere.

Empirical models of the short wave spectrum have been recently developed (e.g. Apel 1994; Elfouhaily et al. 1997) and are based on the functional approximation of measurements. For instance, Apel paid a special attention to the correct description of the capillary-gravity range of the wave spectrum as reported by Jähne and Riemer (1990) in their laboratory experiments. While Elfouhaily et al. explicitly constrained their spectrum to conform to Cox and Munk's (1954) slick and clean surface slope measurements. These models provide a one-way coupling with the atmosphere: they allow to calculate momentum flux to waves but do not provide the dynamical coupling with the atmosphere.

To build a dynamical coupled model wind waves-atmosphere a physical model of the short gravity and capillary-gravity wave spectrum is more appropriate, as it will potentially describe the physical properties of the sea surface under the joint action of wind and surface currents. These models are based on the solution of the energy spectral density balance equation which describes the growth, evolution and decay of waves due to different physical processes. Assuming that the wind input, wave-wave interactions and the dissipation due to wave breaking are proportional to each other in the equilibrium range of the wave spectrum Phillips (1985) obtained the wave variance spectrum S in the form $S(k) \sim (u_*/c)\, k^{-4}$ (k is the wave number and c is the phase speed) which corresponds to measurements of Toba (1973). The similar spectrum was derived by Kitaigorodskii (1983), and Zakharov and Zaslavskii (1982) on the basis of a rather

different assumption: in the equilibrium range the energy input from the wind is assumed to occur primarily at the energy containing scales with dissipation restricted to much shorter scales.

Donelan and Pierson (1987) assumed that in the short gravity and capillary ranges the wave-wave interactions can be neglected. The wave spectrum results from the balance of the wind input and the energy dissipation due to small scale breaking and viscosity. However, such a spectrum underestimates the energy level of the capillary waves as compared to data of Jähne and Riemer (1990). Such a discrepancy may result from the fact that the energy is supplied to the capillary range is not due to the wind input but mainly due to a nonlinear mechanism in which the capillary waves (so called parasitic capillaries) are generated on the crests of steep short gravity waves. In Donelan and Pierson (1987) this mechanism has been neglected.

The principle role of this mechanism in the capillary wave dynamics was demonstrated theoretically by Longuet-Higgins (1963), Ruvinsky et al. (1991) and others, and experimentally by Yermakov et al. (1986), Zhang (1995), and others. These studies have shown that the generation of parasitic capillaries results in effective energy losses by the short gravity waves.

Following Kudryavtsev (1996), in Kudryavtsev et al. (1997) a physical model of the short gravity and capillary wave spectrum is suggested. It is assumed that the balance in the energy spectral density equation results from the wind input, nonlinear wave-wave interactions, energy losses due to wave breaking and the viscous dissipation, and generation of parasitic capillaries by the short gravity waves. This model is used here for dynamical coupling of waves with the atmosphere. The wind input, which supplies the energy and momentum to waves is determined by the friction velocity of the atmosphere, which in turn results from the coupled evolution of wind and waves.

Considering balance equations of sensible heat and humidity in the atmosphere, the surface fluxes of sensible heat and humidity (latent heat flux) can be evaluated in the frame of the wind over waves coupling theory. It has been shown by Makin and Mastenbroek (1996) that, while momentum to a large extent is transported by the organized wave-induced motions correlated with the waves (form drag), heat is transported only by viscosity. The sensible heat and humidity flux above waves is thus determined by the diffusivity of turbulence which is affected by waves. In this case waves have only indirect impact on heat (sensible and latent) fluxes. That explains a well established experimental fact that the sensible heat and humidity exchange coefficients over the sea are much less dependent on the wind speed than the drag coefficient (Anderson 1993; DeCosmo et al. 1996; Friehe, Schmitt 1976; Geernaert 1990; Katsaros et al. 1987, 1994; Large, Pond 1982; Smith 1980, 1988, 1989).

However, waves can directly influence sensible heat and humidity fluxes. Waves break. They eject spray into the atmosphere. The spray droplets evaporate and can change the balance of sensible heat and moisture in the marine surface boundary layer. An additional term, related to the evaporation of droplets, appears in the balance equations for heat and humidity. This term is 'wave-induced' and is analogous to the form drag term in the balance equation for momentum above waves. If this wave-induced, or better to say, the spray mediated sensible heat and humidity flux can become comparable to a direct turbulent flux, then sea spray will play an important role in the exchange processes of sensible heat and moisture.

The effect of the evaporating droplets on heat and humidity transfers in the marine surface boundary layer is determined by the evaporation function. The evaporation function is calculated from the droplets concentration above sea waves. The droplets concentration is related to the bubble production at the sea surface, and the latter to the whitecap coverage of the sea. The whitecap coverage can be calculated directly from the wave spectrum, via the dissipation due to breaking function.

In this way the heat fluxes in presence of sea spray can be calculated from the properties of the sea surface (wave breaking) and peculiarities of the momentum exchange above waves, i.e. they are incorporated into the coupled system waves-atmosphere.

The evolution of the coupled system is then assessed. It is shown that the dynamical coupled model of surface waves- atmosphere allows to obtain correct description of the air-sea interaction. The spectral and integral characteristics of the model wave spectrum agree well with data of the laboratory and field measurements of Jähne and Reimer (1990), Hara et al., (1997), and Cox and Munk (1954). The atmosphere parameters such as the sea drag, the sensible heat and humidity exchange coefficients, and the coupling parameter agree well with field and laboratory measurements of Anderson (1993), Banner and Peirson (1996), Donelan and Pierson (1987), Large and Pond (1982), Smith (1980).

4.2 Wind over waves coupling

The lowest part of the marine surface boundary layer, the so-called wave boundary layer or WBL is considered. The upper boundary of the WBL is defined at the height where all wave-induced fluxes in the atmosphere are negligible. The wave-induced velocities of a wave component with the wave length λ, the wave number $k = 2\pi/\lambda$, and the phase speed c decay on a scale $z \sim k^{-1} \sim c^2/g$. For a fully developed sea, the phase speed at the spectral peak is $c_p \sim u_{10}$, where u_{10} is a wind speed at 10 m height. Thus for a wind speed of 10 m s^{-1}, the decay scale is 10 m. The wave-induced momentum flux which above waves is quadratic in the wave-induced velocities (Phillips 1966) decays much faster. That suggests that a height h of 10 m is a good estimate of the upper boundary of the WBL.

The adjustment time of the turbulent boundary layer T_a is determined by its characteristic height h and the friction velocity u_*, $T_a \sim h/u_*$. For h ~10 m and u_*~0.1 m s^{-1}, we obtain T_a ~100 s. The evolution time of the sea wave field is a few hours (Komen et al., 1994), and thus is much longer than T_a. That means that the WBL can be treated as stationary.

It is further assumed that the wind direction coincides with the mean direction of wave propagation and the wave field (wave spectrum) is symmetrical relative to that direction.

The conservation of the mean momentum in the WBL then reads

$$\frac{\partial \tau}{\partial z} = 0 \qquad (4\text{-}1)$$

which implies that, if the wind is statistically steady and spatially homogeneous, the total stress τ is independent of height.

The total stress is supported by the mean turbulent stress $\tau^t = -\overline{u'w'}$, the wave-induced stress τ^w due to the organized wave motions in the atmosphere induced by waves, and the viscous stress τ_v

$$\tau = \tau^t(z) + \tau^w(z) + \tau^v(z) = \text{Const.} = u_*^2 \tag{4-2}$$

By definition the total stress equals the square of the friction velocity u_*^2. Equation (4-2) was apparently first introduced by Phillips (1966). The viscous stress is important only very near the water surface. Far above the water the wave-induced stress vanishes and

$$\tau = \tau^t = u_*^2 . \tag{4-3}$$

As was stated by Phillips (1966), page 93, *"the interchange between* τ^t and τ^w (we add also τ_v) *as the surface is approached, and the relation between* τ^w and the momentum flux to the waves are the central questions in this whole problem" (the coupling between wind and waves).

The explicit description of fluxes as the wave surface is approached dictates the use of a vertical coordinate system which follows the instantaneous water surface $z = \eta(\vec{x}, t)$, e.g.

$$\hat{z} = h\frac{z - \eta}{h - \eta}. \tag{4-4}$$

The mean space averaged variable is defined in $(\vec{x}, \hat{z})$ coordinate system by the following procedure

$$f(\hat{z}) = \frac{1}{L}\int_0^L \bar{f}(\vec{x}, \hat{z})\, d\vec{x}, \tag{4-5}$$

where $\bar{f}$ is any ensemble *phase* averaged variable (see e.g. Mastenbroek et al. 1996), and L is the averaging distance. The problem of averaging process in the air-sea interaction studies is described, e.g., in Donelan (1990). The averaging process, in our case the waves, must be contained within the space scale of the average, and this scale must be much smaller than the scale of air flows that drives the waves. The estimated averaging time scale for air- sea studies appears to be about 1000 sec (Donelan 1990). The characteristic distance/time of the wave process is the wave length/period of the wave component in the peak of a wave spectrum. For a fully developed sea that is about 100 m and about 10 sec. So, the averaging distance L is about 10^4 m.

The procedure (4-5) is defined in the domain $0 \le \hat{z} \le h$. ($\eta \le z \le h$). Note, that $\hat{z} = 0$ corresponds to the instantaneous water surface $z = \eta$. Hereafter the circumflex above z is dropped.

4.2.1 VISCOUS STRESS

Except very near the water surface, in the viscous sublayer, the viscous stress can be neglected. However, if we want to relate the wave-induced stress directly to waves, and

avoid parameterization of the short waves in terms of a Charnock type relation, the viscous stress has to be accounted for in the description of the momentum flux near the surface.

The sea state in a wind over waves coupling theory is described in terms of the directional wave number spectrum which is defined in the whole range of wave numbers. Introducing the statistical description of waves in terms of the directional wave spectrum it is assumed that all undulations of the water surface can be considered as waves.

If waves are not actively involved in breaking, the instantaneous water surface is a smooth surface and the viscous sublayer always covers the undulating water surface, i.e. waves. It means that the tangential stress at the surface $z = 0$ is supported by molecular viscosity, e.g. the total stress at the surface is $\tau = \tau^w(0) + \tau_v(0)$. To avoid the explicit description of the stress within the viscous layer we shall use a classical parameterization of the viscous layer by introducing the viscous roughness scale (Townsend 1956; Monin, Yaglom 1971):

$$z_0^v = 0.1\frac{\nu}{u_{*0}^l} \tag{4-6}$$

where ν is the kinematic viscosity of the air, and $u_{*_0}^l$ is the friction velocity at the top of the viscous sublayer. The viscous stress in (4-2) can be now neglected

$$\tau^t(z) + \tau^w(z) = u_*^2 , \tag{4-7}$$

and the surface momentum is related now to the height $z = z_{0v}$. The friction velocity $u_{*_0}^l$ is related to the local turbulent stress $\tau^t(z_{0v}) = u_*^2 - \tau^w(z_{0v})$ as friction is not supported by the form drag at the surface $\tau^w(0) = \tau^w(z_{0v})$

$$u_{*0}^l = u_* \sqrt{1 - \frac{\tau^w(0)}{u_*^2}}. \tag{4-8}$$

The ratio

$$\alpha_c = \frac{\tau^w(0)}{u_*^2} \tag{4-9}$$

is called the coupling parameter. The coupling parameter shows which part of the total stress at the surface is supported by the form drag. It is bounded by the condition $\alpha_c < 1$.

The parameterization of the viscous stress above the wave surface in the form (4-6) is possible if the very short waves with lengths $\lambda < \delta_v \sim \nu/u_*^l$ do not contribute to the wave-induced flux τ^w, or, in other words, that the wave-induced stress is constant within the viscous sublayer δ_v. These scales are so small, that capillaries are already damped by viscous dissipation (Donelan, Pierson 1987; Elfouhaily et al. 1997; Jähne, Riemer 1990).

The assumption that the instantaneous water surface is a smooth surface is a crucial one. It could be argued that except at low wind speeds breaking always occurs in the

ocean, and the water surface is blurred. And that is true. Breaking is a highly nonlinear local process which disrupts the water surface. However, if the process is weak-in-the mean, as in the formalism widely used in the description of sea waves (Hasselmann 1968), the instantaneous water surface can be regarded in the mean as a smooth one. Using for the instantaneous fraction of the sea surface covered by whitecaps relation

$$W(u_{10}) = 3.84 \times 10^{-6} u_{10}^{3.41} \tag{4-10}$$

(e.g. Monahan et al. 1986) one can find the whitecap coverage of 1%, 4 %, 10% and 22% of the sea surface for the corresponding wind speed of 10 m/s, 15 m/s, 20 m/s and 25 m/s, which supports the weak-in-the mean assumption for the wave breaking.

Notice, that in the above description the *instantaneous* water surface is distinguished from the *sea surface*. The latter, being viewed from a distance far above waves, is a rough surface due to the presence of waves.

4.2.2 TURBULENT STRESS

The local closure, eddy-viscosity K theory, which relates the turbulent flux to the gradient of the associated mean variable is used here

$$\tau^t(z) = K\frac{\partial u}{\partial z}. \tag{4-11}$$

From (4-7) and (4-11)

$$K\frac{\partial u}{\partial z} = u_*^2 - \tau^w(z). \tag{4-12}$$

The surface boundary condition is $u = 0$ at $z = z_0'$ and the velocity profile above waves follows immediately from (4-12)

$$u(z) = u_*^2 \int_{z_0'}^{z} \left[1 - \frac{\tau^w(z)}{u_*^2}\right] K^{-1} dz. \tag{4-13}$$

The eddy-viscosity $K(z)$ above waves will be estimated from the balance equation of the turbulent kinetic energy (TKE).

4.2.3 BALANCE EQUATION OF THE TKE

The balance equations of the TKE e in the atmosphere reads:

$$-\frac{\partial}{\partial z}\overline{(e' + p')w'} + P - \varepsilon = 0 \tag{4-14}$$

where the first term on the left hand side is the diffusive transport of the TKE, P is the production of the TKE, and ε is the dissipation rate to heat.

The diffusive transport of the TKE in the balance equation above waves can be neglected, and the balance equation reduces to (Chalikov, Belevich 1993; Makin, Mastenbroek 1996)

$$P = \varepsilon, \tag{4-15}$$

which says that the production of the TKE P equals its dissipation to heat ε. The production of the TKE P above waves has two contributions: production by interaction of the turbulent stress and the mean velocity shear

$$P^t = \tau^t \frac{\partial u}{\partial z}, \tag{4-16}$$

and by interaction of the wave-induced turbulent stress $\tilde{\tau}^t$ and the mean (averaged by the procedure (4-5) wave-induced velocity shear

$$P^w = \left\langle \tilde{\tau}^t \frac{\partial \tilde{u}}{\partial z} \right\rangle \tag{4-17}$$

where~ denotes a wave-induced fluctuation, and brackets indicate the average (4-5) for a second moment. The total production above waves is thus

$$P = P^t + P^w. \tag{4-18}$$

The production terms P^t and P^w represent the transfer of kinetic energy from the mean and mean wave-induced motions to the turbulent motion. They appear with the opposite sign as the sink terms in the equations for the kinetic energy of the mean $E = u^2/2$ and mean wave-induced $E_w = \langle \tilde{u}^2 + \tilde{w}^2 \rangle / 2$ motions.

The balance equation of E can be derived from (4-1) by multiplying it by u (the time derivative is kept here) and accounting for (4-7):

$$\frac{\partial E}{\partial t} = \frac{\partial}{\partial z} u(\tau^t + \tau^w) - \tau^t \frac{\partial u}{\partial z} - \tau^w \frac{\partial u}{\partial z}. \tag{4-19}$$

The first term on the right hand side describes the transport of E, the second term is the sink of the mean energy into the TKE P^t, the third term describes the mutual transfer of energy between the mean and the wave-induced motions. It appears with the opposite sign in the balance equation of the mean wave-induced energy E_w, where the vertical flux of the wave-induced energy is neglected (see Makin, Mastenbroek 1996)

$$\frac{\partial E_w}{\partial t} = \tau^w \frac{\partial u}{\partial z} - P^w. \tag{4-20}$$

For a growing wind wave field $\tau^w > 0$ and this term describes the sink of the mean energy into the mean wave-induced energy.

In stationary conditions the TKE production above waves is thus

$$P = P^t + P^w = (\tau^t + \tau^w)\frac{\partial u}{\partial z} = u_*^2 \frac{\partial u}{\partial z}. \quad (4\text{-}21)$$

Using the mixing length theory and expressing the dissipation in terms of K and the mixing length $l = \kappa z$, $\varepsilon = K^3 l^4$, the equation for the eddy-viscosity is found from (4-15) and (4-21)

$$K(z) = l u_* \left(1 - \frac{\tau^w(z)}{u_*^2}\right)^{1/4}. \quad (4\text{-}22)$$

4.2.4 WAVE-INDUCED STRESS

If the sea surface is assumed to be a superposition of random waves of all scales, characterized by a directional wave spectrum $S(k, \phi)$ (k is the wave number which satisfies the gravity-capillary dispersion relation, ϕ is the propagation direction of the k-wave component relative to the wind direction), the wave-induced stress can be written

$$\tau^w(z) = \tau^w(0) f(z), \quad (4\text{-}23)$$

where $\tau^w(0)$ is the form drag

$$\tau^w(0) = \int_0^\infty T(k)\, d(\ln k), \quad (4\text{-}24)$$

and T is the omni-directional spectrum of the momentum flux to waves

$$T(k) = \int_{-\pi}^{\pi} c^2 B(k,\phi)\, \beta(k,\phi) \cos\phi\, d\phi, \quad (4\text{-}25)$$

$B(k,\phi) = k^4 S(k,\phi)$ is the saturation wave spectrum, $\beta(k, \phi)$ is the growth rate parameter describing the energy flux to waves from the atmosphere, and $f(z)$ is a dimensionless function describing the vertical decay of the mean wave-induced stress. Function f is defined as

$$f(z) = \frac{1}{\tau^w(0)} \int_0^\infty T(k)\, F(k,z)\, d(\ln k) \quad (4\text{-}26)$$

where $F(k,z)$ is a dimensionless function describing the vertical distribution of the wave-induced flux of the individual wave components and satisfying the condition $F(k, z_{v_0}) = 1$.

4.2.5 GROWTH RATE PARAMETER

In Makin et al. (1995), Makin (1997) it was shown that the short gravity-capillary and gravity waves (in the centimetre to meter wave length range) play the dominant role in supporting the form drag (and thus the sea drag) at high winds at the surface. Waves longer than 10 metre support only about 10% of the form drag. Thus the accurate estimation of the growth rate parameter for short slow moving waves is required.

In the present the widely accepted parameterization of the growth rate parameter for the short waves remains the parameterization of Plant (1982), which is based on several laboratory and field measurement, and have the form

$$\beta = c_\beta \left(\frac{u_*}{c}\right)^2 \quad (4\text{-}27)$$

where an empirical constant $c_\beta = 32 \pm 16$. Recent analytical theory of the wave growth, based on a rapid distortion theory of turbulence above waves, (Belcher, Hunt 1993), and numerical solution of the Reynolds equations with a second-order turbulent closure scheme (Mastenbroek et al. 1996; Mastenbroek 1996) support the fact that the growth rate parameter is proportional to $(u_*/c)^2$ for waves travelling slower than the wind.

4.2.6 NUMERICAL SIMULATIONS

In Figure 4.1 numerical calculations of the air flow above a sinusoidal wave, based on the model of Mastenbroek et al. (1996), for the range of the external parameters relevant for the present study are shown. The solution of the model depends on three dimensionless parameters being the inverse wave age u_λ/c, dimensionless roughness kz_0 or equivalently the initial drag coefficient $c_\lambda = \kappa^2/\ln^2(k\lambda/kz_0)$ (the velocity and the drag coefficient are related to the height $z = \lambda$) and the wave slope ak. Parameters u_λ/c and c_λ are varied, while the slope is kept constant $ak = 0.01$. Though there are small variations in c_β in the range of parameters considered, the numerical results show that c_β can be well approximated by a constant. The most striking feature is that the numerical values of c_β, though agree well with the analytical solution of Belcher and Hunt (1993) (see Mastenbroek et al. 1996), are twice lower than the mean value of Plant's parameterization $c_\beta = 32$. This discrepancy is the feature of all wave wind generation theories and is not yet understood. However, an important conclusion is that both experiment and theory show that the growth rate β scales with the square of the friction velocity $(u_*/c)^2$.

4.2.7 SCALING FRICTION VELOCITY

In a theory of wind over waves coupling the turbulent stress changes with height above waves and so does the *local* friction velocity $u_*^l(z) = (\tau^t(z))^{1/2}$ (the *total* friction velocity u_*, equations (4-2) and (4-7), is constant over height!).

According to Makin et al. (1995), Makin (1997) the coupling parameter α_c can reach a value of about 0.8 for high wind speeds. From (4-8) it means that the friction velocity

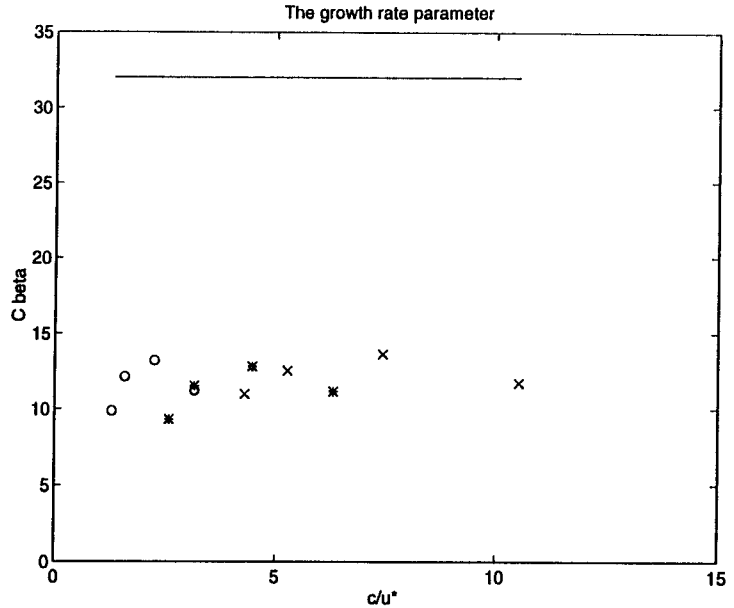

Figure 4.1 c_β, equation (4-27), as function of wave age c/u_*. Inverse wave age parameter u_λ/c equals 3 (crosses), 5 (stars), 10 (circles). The initial drag coefficient 10^3 c_λ is 1, 2, 4 and 6. Wave slope ak = 0.01. The mean value of c_β= 32 according to Plants' parameterization is shown by line.

at the water surface is only 50% of the total friction velocity. Which friction velocity has to be used in scaling the growth rate β in equation (4-27)?

As analytical theories presume the friction velocity which does not change with height, while the numerical studies are usually done for waves of a small or moderate amplitude when the local friction velocity changes only little with height (< 1 % above waves with ak = 0.01, this study, and about 5% above waves with ak= 0.1, e.g. Gent and Taylor (1976), Makin (1990)), the question was not risen before.

The following numerical experiment was designed. The air flow is simulated above slow u_λ/c=5 steep waves with slopes up to ak = 0.3. Above steep waves the pronounced changes with height (up to 30%) of the friction velocity are developed (Makin 1990). The calculated values of the growth rate are then scaled with the total friction velocity u_* and with the friction velocity u_*^l at the vicinity of the surface. Results are presented in Figure 4.2. The conclusion is clear, parameter c_β remains close to a constant being scaled with the surface friction velocity. The physical explanation to that fact follows from the wave growth theory of Belcher and Hunt (1993). According to this theory the growth of waves results from an asymmetric pressure perturbation at the wave surface, caused by the action of the Reynolds shear stress inside the inner region - a thin region adjacent to the wave surface. When the Reynolds stress is varied with height (in our case this variation is caused by the large wave slope) it is logical to use

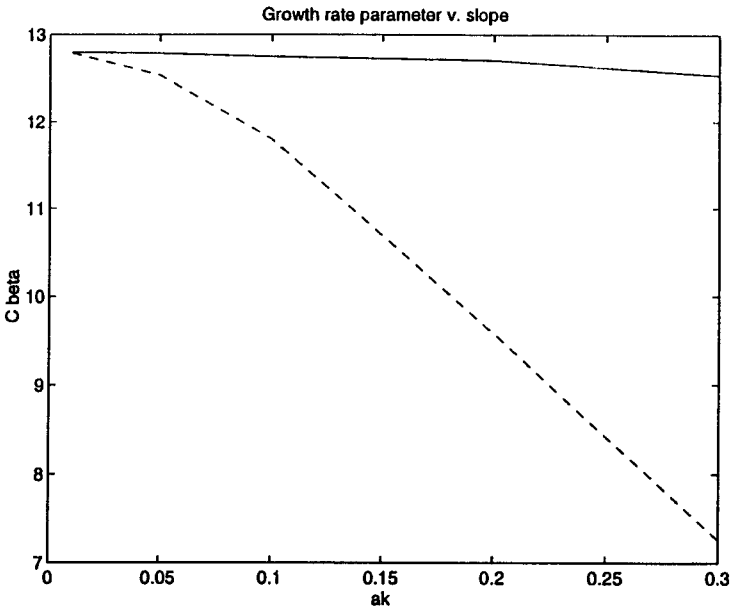

Figure 4.2 c_β as a function of wave slope ak. u_λ/c= 5 , 10^3 c_λ =2 . Dashed line - scaling with the total friction velocity, equation (4-27); solid line - scaling with the local friction velocity, equation (4-28).

the value of friction velocity inside the inner region as a principle parameter in parameterization of the growth rate parameter. The expression (4-27) for the growth rate β can be rewritten

$$\beta = c_\beta \left(\frac{u_*^l(\delta)}{c} \right)^2 . \qquad (4\text{-}28)$$

The height of the inner surface layer δ is proportional to the height of the inner layer L and the roughness length z_0, $\delta \sim (Lz_0)^{1/2}$. The height of the inner region of the wave component k is defined by $k\,L = (2\kappa u_*)/|u_l - c|$ (see Belcher, Hunt 1993). Rough estimates for these heights are k ~0.1 and $k\,\delta$~0.01 (Mastenbroek et al. 1996). Notice, that for short slow waves $\delta \to z_0^l$ and $u_*^l(\delta) \to u_*(1-\alpha_c)^{1/2}$, while for fast waves $\delta \to h$ and $u_*^l(\delta) \to u_*$. Relation (4-28) is valid for the growth rate of monochromatic waves. If the sea surface is presented as a sum of many wave spectral components the local friction velocity $u_*^l(\delta)$ is not constant over the height inside the inner surface layer of a certain wave component. In this case the local friction velocity should be replaced by the friction velocity averaged over the surface boundary layer from z_0^l to $\delta(k)$. We define this averaged friction velocity $(\overline{u_*^l})^2$ as

$$(u_*^l)^2 = \int_0^\infty (u_*^l)^2 e^{-z/\delta} d(z/\delta) = u_*^2 (1 - \alpha_c \bar{f}(k)) \qquad (4\text{-}29)$$

where $\bar{f}(k)$ is the averaged over the surface boundary layer dimensionless wave-induced stress

$$\bar{f}(k) = \int_0^\infty f(z)\, e^{-z/\delta} d(z/\delta) \tag{4-30}$$

and f is defined by (4-26). Hence, we rewrite relation (4-28)

$$\beta = c_\beta \left(\frac{u_*}{c} \right)^2 \left[1 - \alpha_c \bar{f}(k) \right] \cos\phi |\cos\phi|. \tag{4-31}$$

To account for waves travelling at the angle to the wind the angular dependence of β is introduced in (4-31). The angular dependence follows from the numerical study of Mastenbroek (1996).

An important conclusion which follows from (4-31) is that Plant's constant c_β defined by relation (4-27) for short waves is not a constant, but depends on the coupling parameter α_c. This fact can partially explain the scatter in measurements of c_β.

It is a known fact that for fast moving waves the growth rate reduces to zero (experiment of Snyder et al. (1980), numerical simulations of Mastenbroek et al. (1996), analytical theory of Hunt et al. (1997)) so that the parametrization (4-31) in the vicinity of $u_{10} \sim c_p$ becomes invalid. The experimental estimate of the growth rate for fast moving waves was obtained by Snyder et al. (1980) in the range of $1 < u_5/c < 4$, where the wind velocity is taken at 5 metre height,

$$\beta = 0.25 \left(\frac{u_5}{c} - 1 \right). \tag{4-32}$$

To account for the fact that the growth rate for the fast moving waves tends to zero the correction of $C_\beta = m_\beta R$ is introduced, where m_β is a constant

$$R = 1 - 1.3 \left(\frac{c}{u_{10}} \right)^5 \tag{4-33}$$

For slow moving waves $R \sim 1$ and the Plant parameterization is recovered, for fast moving waves $R \to 0$ and $\beta \to 0$.

Finely for waves moving faster than the wind ($R < 0$) the parameterization of β follows from the fact that the energy flux to such waves is mainly due to the tangential stress $\dot{E} = \langle \tau^t u_\Omega \rangle$ (Mastenbroek 1996), where u_0 is the orbital velocity. As $\tau^t \sim (u - u_0)^2$, $u_0 \sim akc$, $c_d^{1/2} = u_*/u$ and with $\beta = \dot{E}/\omega E$ we obtain

$$\beta \sim -c_d^{1/2} \frac{u_*}{c}. \tag{4-34}$$

Writing (4-34) in the form (4-27) we obtain $c_\beta \sim c/u_{10} \sim 1$, which is much smaller than for slow waves, and β for waves travelling faster than the wind in principle can be set to zero.

The final parameterization of β used throughout the study has the form (4-31), where c_β is redefined as

$$c_\beta = m_\beta \max(0, R). \tag{4-35}$$

m_β is treated as a tuning constant in the wind over waves coupled model. In Makin and Kudryavtsev (1997) it was shown that the value of m_β matches exactly the mean value of 32 of Plant's parameterization (4-27).

4.2.8 VERTICAL DECAY FUNCTION

The vertical decay function $F(k,z)$ in equation (4-26) defines the vertical distribution of the wave-induced flux. It seems that the natural decay for the second wave- induced moment should be at least $F(k,z) = \exp(-2kz)$, as the first moment (velocity components) decays as $\exp(-kz)$ in the potential flow. However the rapid distortion theory of turbulence above waves (Belcher, Hunt 1993) suggests another decay length - the height of the inner region L as a result of smearing of the wave fluctuations of turbulent stresses in the outer region. In the outer region the turbulent eddies are rapidly distorted and the wave-induced turbulence is not in local equilibrium with shear. The wave-induced turbulent stress $\tilde{\tau}^t$ is suppressed and the wave-induced motion is close to inviscid and potential. The mean wave-induced flux is thus suppressed too in the outer region. The vertical decay of the wave- induced stress can be parametrized as

$$F(k,z) = e^{-z/L}. \tag{4-36}$$

In Figure 4.3 the decay function $F(k,z)$ for a slow moving wave is shown. The numerical result supports the fact that the height of the inner region is the decay length of the wave- induced flux. The vertical oscillatory decay behaviour of the flux reflects the nature of the oscillatory flow caused by the orbital velocities in the viscous fluid. The numerical solution is approximated by

$$F(k,z) = e^{-z/L} \cos\left(\frac{\pi}{2} \frac{z}{L} \right) \tag{4-37}$$

4.3 Resistance law above waves

From (4-13) and (4-22) the wind profile above waves can be now written

$$u(z) = \frac{u_*}{\kappa} \int_{z_0^V}^{z} \left[1 - \frac{\tau^w(z)}{u_*^2} \right]^{3/4} d(\ln z). \tag{4-38}$$

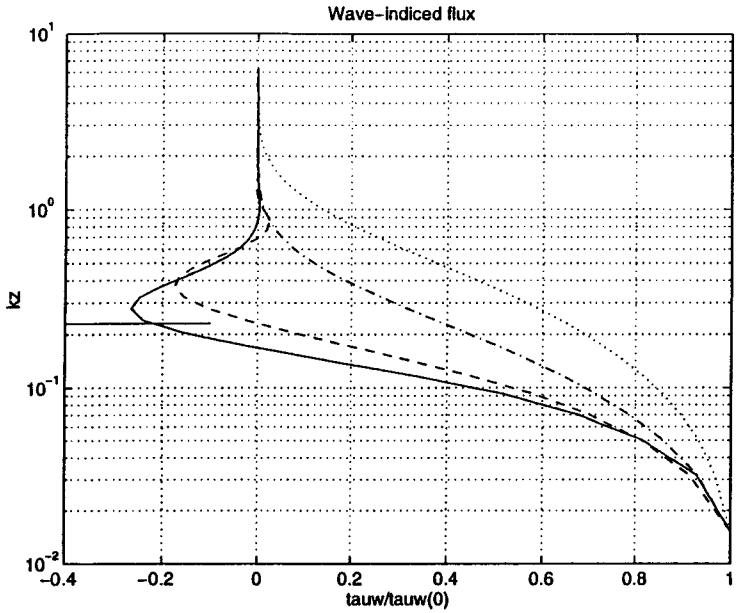

Figure 4.3 The vertical decay function $F(k,z)$ of the wave- induced flux for a slow moving wave (u_λ/c= 10 , 10^3 c_λ =2). Dotted - potential decay exp(-2kz), dashed-dotted - decay at the height of the inner region exp($-z/L$), solid - numerical calculation, dashed – approximation (4-37).

The resistance law in terms of the drag coefficient $C_D=u_*^2/u_{10}^2$ follows from (4-38) and (4-9)

$$C_D^{1/2}=\frac{u_*}{u_{10}}=\kappa\left(\int_{z_0}^{10}\left[1-\alpha_c f(z)\right]^{3/4} d(\ln z)\right)^{-1}. \qquad (4\text{-}39)$$

and the coupling parameter is expressed via (4-34)

$$\alpha_c=\frac{1}{u_*^2}\int_0^\infty T(k)\,d(\ln k) \qquad (4\text{-}40)$$

Relation (4-39) is fundamental in a sense that it relates the drag of the sea surface directly to the properties of the momentum exchange at the surface via the coupling parameter (4-40) and the vertical distribution of the wave-induced stress $f(z)$. The coupling parameter is determined by the geometrical properties of the surface via the directional wavenumber wave spectrum $S(k,\phi)$ and by peculiarities of energy exchange between wind and waves.

The wind over waves coupled model, described above, is in fact a higher order parameterization of the marine atmospheric surface boundary layer, compared to the traditional bulk parameterization. The wind over waves coupling relates the sea drag directly to the geometrical properties of the sea surface via the wavenumber directional wave spectrum and properties of momentum exchange at the sea surface.

Equations (4-39) and (4-40) can be solved by iterations after the form of a wave spectrum $S(k, \phi)$ is given by a functional relation or is specified by a physical model based on the solution of the wave energy balance equation.

4.4 Spectrum of short waves

The physical model of the short gravity and capillary wave spectrum, used in the present wind over waves coupling theory is developed in Kudryavtsev (1996), and further in Kudryavtsev et al. (1997). The model is based on the energy balance equation where the balance of the wave spectral energy results from the wind input, dissipation due to viscosity and wave breaking, nonlinear interactions, and generation of parasitic capillaries by steep short gravity waves.

4.4.1 ENERGY BALANCE EQUATION

Assuming that the wave field is statistically steady and spatially homogeneous, the local balance of the wave energy spectral density $E(k,\phi)$ is written in the form

$$\frac{\rho_a}{\rho_w}\beta\omega E-4\nu_w k^2 E+D-\nabla\bullet\vec{T}=0. \qquad (4\text{-}41)$$

The first term on the l.h.s. is the wind input written in terms of the growth rate parameter β, the second term describes the energy losses due to the viscous dissipation (ν_w is the kinematic water viscosity); D is the wave dissipation due to wave breaking and generation of the parasitic capillary waves, P is the source of the nonlinear generation of capillary waves by the steep short gravity waves, and$\nabla\bullet\vec{T}(\vec{k})$ represents the net spectral flux of energy through the wave number k by the resonant wave-wave interactions. The energy spectrum is related to the wave variance spectrum $S(k,\phi)$, which characterize the statistical properties of the sea surface, by the relation

$$E(k,\phi)=\frac{\omega^2}{k}S(k,\phi), \qquad (4\text{-}42)$$

where the wave frequency ω and the wave number k satisfies the dispersion relation

$$\omega^2=gk+\gamma k^3 \qquad (4\text{-}43)$$

(g is the acceleration of gravity, and γ is the kinematic surface tension of the water).

4.4.2 WIND INPUT

The parameterization of the growth rate parameter $\beta(k,\phi)$ is given by relation (4-31) and (4-35) and for convenience is rewritten here

$$\beta(k,\theta) = c_\beta\left[1-\alpha_c\bar{f}(k)\right]\left(\frac{u_*}{c}\right)^2\cos\phi|\cos\phi|, \tag{4-44}$$

For short waves $c_\beta = m_\beta \bar{f}(k) \to 1$ and (4-112) reduces to

$$\beta(k,\theta) = m_\beta\left[1-\alpha_c\right]\left(\frac{u_*}{c}\right)^2\cos\phi|\cos\phi| \tag{4-45}$$

As expressed, (4-45) differs from the 'classical' parameterization of Plant (1982), relation (4-27), by a factor $(1-\alpha_c)$. Parameterization of β via the surface stress $(1-\alpha_c)$ u_*^2 can be explained by the sheltering theory of the wave growth (Belcher, Hunt 1993), where the energy flux to waves results from the dynamics of turbulent wave-induced stresses in a very thin layer adjusted to the wave surface.

4.4.3 GENERATION OF PARASITIC CAPILLARY WAVES

It is well known, that short gravity waves (SGW) (wave length 0.03-0.3 m) approaching their maximum steepness generate 'parasitic' capillary waves (CW) on their forward face (Longuet-Higgins 1963; Phillips 1966; Crapper 1970; Ruvinsky et al. 1991). These capillaries are well observed in the laboratory experiments (Chang et al. 1978; Yermakov et al. 1986). They originate from the work of a pressure impulse connected with locally large value of the curvature of the SGW crest. As the group velocity of the CW exceeds the phase velocity they travel along the forward face of the SGW and disappear due to the molecular viscosity.

Parameterization of the term P which describes the generation of the parasitic capillary waves in the balance energy equation (4-21) was developed in Kudryavtsev (1996) (see also Kudryavtsev et al. 1997), and is based on general assumption that short gravity waves lose their energy due to generation of parasitic capillaries. The nonlinear losses of the SGW energy at the wavenumber K generate the parasitic capillary wave at wavenumber k, which in turn dissipates due to molecular viscosity. The wave numbers K and k satisfies the relation

$$k = \frac{g}{\gamma K}. \tag{4-46}$$

In spectral terms the cascade energy flux from the SGW spectral domain $kdkd\phi$ is balanced by the viscous dissipation of the CW energy, which is concentrated in the spectral domain $kdkd\phi'$. This nonlinear flux results in the dissipation of the SGW energy

$$D(K\phi) = P(k,\phi')\frac{kdkd\phi}{KdKd\phi} \tag{4-47}$$

As a train of the parasitic capillaries is parallel to the crests of carrying SGW (see e.g. Yermakov et al. 1986; Zhang 1995), the band of the SGWs propagating in the range $d\phi$ generates a train of the CWs within the same range of directions, i.e. $d\phi'=d\phi$. From (4-46)

$$\frac{KdKd\phi}{kdkd\phi'} = \left(\frac{k_c}{k}\right)^4 \tag{4-48}$$

where $k_c = (g/\gamma)^{1/2}$ is the wavenumber corresponding to a minimum of the phase speed. The source of parasitic CWs in the balance equation (4-111) takes the form:

$$P(k,\phi) = \left(\frac{k_c}{k}\right)^4 D(K,\phi) \tag{4-49}$$

The dissipation of the SGW is taken at the wavenumber $K = k_c^2/k$. Equation (4-49) gives an explicit relation for the nonlinear generation of the parasitic capillaries source term P in the balance energy equation (4-111).

The parasitic capillaries can not be generated effectively by all gravity waves. It was reported in Yermakov et al. (1986), that even in the laboratory conditions they could not observe trains of the parasitic CWs on the SGW with the wave length longer than 30cm. In real conditions, crests of the decimeter gravity waves break rather than generate the trains of capillaries. Hence, if we assume that SGWs with the wave length longer than 10-15 cm do not generate the CWs, but break and lose their energy to generate the turbulence, then the applicability of (4-49) is restricted by the wavenumber range of k ~2000-3000 rad/m.

4.4.4 ENERGY DISSIPATION DUE TO WAVE BREAKING

Wave breaking is a rather rare event on the sea surface. Hence, wave breaking is a local process in physical space, but a distributed process in Fourier space (Phillips 1985). The parameterization of dissipation due to breaking follows the approach of Phillips (1985) with some modifications suggested in Kudryavtsev et al. (1997).

Duncan (1981) experimentally studied the energy loss which occurs in one "individual" wave breaker. He has shown that the shape of breakers is geometrically similar for waves of different scales. The rate of energy loss D per unit surface in a breaker moving with the phase speed c was found to be:

$$D = bc^3, \tag{4-50}$$

where b is an empirical constant of order 0.01. The wave number of the wave carrying a breaker is identified by its phase speed $c = g/k^2$.

Following Phillips (1985) a statistical distribution of characteristics of breakers, namely the density of frequency of wave breaking events $N(\hat{c})$ passing a given point at the surface with velocities of advance between $\hat{c}$ and $\hat{c}+d\hat{c}$ is considered. The expected number of breakers passing a given point per unit time is then $N(\hat{c})\,d\hat{c}$. With (4-50) the average rate of the energy dissipation of waves by breakers with speeds in the range $\hat{c}$ to $\hat{c}+d\hat{c}$ can be written as:

$$<D> = 2\pi b g^{-1} c^4 N(\vec{c})\, d\vec{c}. \qquad (4\text{-}51)$$

When every wave crest in the wave field breaks the quantity $2\pi/g\, cN(\vec{c})\, d\vec{c}$ is close to 1 and equation (4-51) reduces to (4-50). At sea the fraction of wave crests carrying a breaker is small in general. That means that although the energy of a breaking wave is concentrated in a small are $ad\vec{k}\,d\omega$ around the point $\omega = g/c$, $\vec{k} = (g/c)^{1/2}\vec{c}/c$, which satisfies the dispersion relation, the rate of energy dissipation $<D>$ is distributed in the frequency - wavenumber space along the line $\omega=(c^2/c_1)\, k_1 = (c^2/c_2)\, k_2$. For simplicity a case when all waves run in the same direction is considered. The fraction of crests carrying breakers is small ($\varepsilon = 2\pi g^{-1} cN(\vec{c})\, d\vec{c} \ll 1$). As the spatial scale of a single breaker is comparable with the half of the wave length (Duncan 1981), it is reasonable to assume that the spectrum of dissipation $Diss(\omega,k)$ has the form of a "white noise" which is distributed along the line $\omega=c\,k$ over an area A equals to

$$A = dc \int_{k^1}^{k^2} k\, dk = \frac{1}{2} g^2 c^{-4} dc, \qquad (4\text{-}52)$$

where the limits of integration are: $k^1=\varepsilon k^2$, $k^2=(g/c)^{1/2}$. The relation for the spectral rate of energy dissipation follows from (4-51) and (4-52):

$$Diss(\omega, k) = <D> A^{-1} = 4\pi b g^{-3} \left(\frac{\omega}{k}\right)^8 N(c) \qquad (4\text{-}53)$$

where $\omega = c \bullet k$ (with given c), and the spectrum $Diss(\omega,k)$ along the k-axis is restricted to the interval $\varepsilon(g/c)^{1/2} < k < (g/c)^{1/2}$.

Relation (4-53) describes the frequency-wavenumber spectral rate of energy dissipation by a narrow band of breaking waves running with the speed in the range c to $c+dc$. Let's assume that the sea surface is presented by a superposition of waves in a wide range of wave numbers. Then the wave number spectrum of energy dissipation $D(k)$ can be found from (4-53) by integration over all frequencies for a given k:

$$D(k) = \int Diss(\omega, k)\, d\omega. \qquad (4\text{-}54)$$

Anticipating that $(\omega/k)^2\, g^{-1} N(c)$ is a slowly varying function of frequency, integration of (4-54) gives

$$D(k) = \frac{4}{7} \pi b g^{3/2} k^{-7/2} N(c). \qquad (4\text{-}55)$$

Relation (4-55) describes dissipation in uni-directional wave train. The angular spreading of energy losses is defined by the number of breakers propagating in the range of directions ϕ to $\phi+d\phi$. Hence, the directional spectrum of energy dissipation obviously results from (4-55) and has the form:

$$D(k, \phi) = \frac{4}{7} \pi b g^{3/2} k^{-9/2} N(c, \phi) \qquad (4\text{-}56)$$

where $N(c,\phi)$ is a 2-D density of the frequency of wave breaking events, so that $N(c,\phi)\, dc\, d\phi$ is the expected number of breakers passing the given point per unit time in the range of speed c to $c+dc$ and in the range of direction ϕ to $\phi+d\phi$. Note that $N(c) = \int N(c,\phi)\phi$. To obtain the final equation for the spectral rate of dissipation the explicit relation for $N(c,\phi)$ should be found. It is assumed, that the frequency of wave breaking events depends on the ratio of the degree of saturation of the wave variance spectrum $B=k^4 S$ to some threshold level α_g:

$$2\pi \frac{c}{\omega} N(c, \phi) = \left(\frac{k^4 S(k, \phi)}{\alpha_g} \right)^{n_g + 1}, \qquad (4\text{-}57)$$

where n_g and α_g are to be defined. Relation (4-57) describes the intensification of the wave breaking when the local degree of saturation approaches the threshold level. The final equation for the spectral rate of energy dissipation by wave breaking is now obtained from (4-56) and (4-57):

$$D(k, \phi) = g^{3/2} k^{-7/2} \left(\frac{B(k, \phi)}{\alpha_g} \right)^{n_g} B(k, \phi). \qquad (4\text{-}58)$$

In deriving (4-58) the term $2b/(7\alpha_g) \sim 1$ is omitted because further the threshold level α_g will be treated as a turning parameter. At $n_g=2$ equation (4-58) corresponds to the rate of dissipation obtained by Phillips (1985). At arbitrary n_g this equation corresponds to the parameterization of the dissipation proposed by Donelan and Pierson (1987). It is interesting to note that though Phillips, and Donelan and Pierson have started from two principally different assumptions concerning the nature of the wave breaking (dissipation is local in physical space and dissipation is local in Fourier space) the final equation has the same functional relation.

In the gravity range of the wave spectrum where the wave energy is lost due to wave breaking and dissipates into turbulence, parameters n_g and α_g are universal constants. However, for the very short gravity waves, in the range of the wave length from several to 10-15 centimeters, the losses of energy is mainly due to the generation of the parasitic capillary waves. If we still assume that the spectral rate of dissipation of these waves is described by equation (4-58), then parameters n_g and α_g should be some functions of the dimensionless wave number $(k^2\, \gamma/g)^{1/2}$ rather than constants.

4.4.5 RESONANT WAVE-WAVE INTERACTIONS

The resonant wave-wave interactions redistribute spectral wave energy in the $\vec{k}$ plane. The resonant four-wave interactions are dominant in the gravity interval of the wave spectrum (Hasselmann 1962). In the capillary-gravity interval the resonant three-wave interactions take place.

The detailed study of the resonant energy flux in the capillary-gravity interval of the spectrum was done by Valenzuela and Laing (1972). They have shown that the three-wave interactions redistribute energy from the vicinity of the wavenumber $k_c=(g/\gamma)^{1/2}$ towards gravity and capillary waves. The 'passive' wave component in the gravity interval $k/k_c < 1$ loses energy to two 'active' wave components in the capillary interval. If the 'passive component is in the capillary interval $k/k_c > 1$ the two active components can be in both gravity and capillary intervals.

The exact expression for the resonant energy spectral flux divergence is given in Valenzuela and Laing (1972). Here a parameterization of the three-wave interactions is used:

$$\nabla\cdot\vec{T} \sim k^5\omega^{-1}E^2(k,\phi) = k^{-5}\omega^3 B^2(k,\phi) \tag{4-59}$$

which follows from the dimensional analysis and the fact that the resonant three-wave interactions are of the second order. In principle, equation (4-59) is not correct, because the three-wave interactions are not local in the wavenumber space. Nevertheless relation (4-59) describes the resonant interactions phenomenologically. It is introduced to account for the nonlinear limitation of the wave growth in the vicinity of $k \sim (g/\gamma)^{1/2}$.

In the gravity interval, far from the spectral peak, the four- wave interactions are local in the wave number space and the spectral flux divergence can be written as (Phillips 1985):

$$\nabla\cdot\vec{T} \sim k^{-5}\omega^3 B^3(k,\phi) \tag{4-60}$$

4.4.6 SHORT GRAVITY WAVE SPECTRUM

The spectrum of short gravity waves results from the balance of wind input, dissipation, and four-wave interactions. With (4-58) and (4-60), the spectral energy balance equation (4-111) takes the form:

$$\beta_v\omega E(k,\phi) - g^{3/2}k^{-7/2}B(k,\phi)\left[\frac{B(k,\phi)}{\alpha_g}\right]^{n_g} + \alpha_n g^{3/2}k^{-7/2}B^3(k,\phi) = 0 \tag{4-61}$$

where $\beta_v = \rho_a/\rho_w\ \beta\text{-}4\ \nu k^2/\omega$ is the difference between the growth rate and the rate of viscous dissipation, and α_n is a constant. Donelan and Pierson (1987) assumed that in the short gravity wave interval the resonant wave interactions play a minor role, so that the shape of their spectrum results from the balance of wind input and dissipation due to wave breaking and viscosity. Their spectrum follows then from (4-61) where the third term is neglected:

$$B(k,\phi) = \alpha_g\left[\beta_v(k,\phi)\right]^{1/n_g}, \tag{4-62}$$

and parameters α_g and n_g are to be determined by fitting the model spectrum to observations.

Unlike Donelan and Pierson (1987), Phillips (1985) considered all three terms to be significant and proportional to each other, which implies that parameter n_g in (4-61) should be equal to 2. In this case the spectral shape is again described by (4-62) but with $n_g = 2$. This spectrum predicts approximately linear dependence of the spectral level on the wind speed, a fact revealed in a number of laboratory experiments (Jähne, Riemer 1990; Hara et al. 1997; Zhang 1995). Therefore the short gravity wave spectrum is taken here in the form

$$B(k,\phi) = \alpha_g\left[\beta_v(k,\phi)\right]^{1/2}, \tag{4-63}$$

As all terms in (4-61) are assumed to be proportional to each other, constant α_n can be inserted in tunining constant α_g. Note, that the angular spreading of $B(k,\phi)$ appears in (4-63) through the angular dependence of the growth rate parameter.

4.4.7 CAPILLARY-GRAVITY WAVE SPECTRUM

In the capillary-gravity interval $k > (g/\gamma)^{1/2}$ the wave spectrum can be obtained from the balance of wind input, viscous dissipation, generation of parasitic capillaries, and 3-wave resonant interactions:

$$\beta_v\omega E(k,\phi) + (k_c/k)^4 D(K,\phi)\ F - \alpha_{cg}\bar{g}^1 k^5\omega^{-1}E^2(k,\phi) = 0 \tag{4-64}$$

where α_{cg} is a constant to be defined; $D(K,\phi)$ is the nonlinear dissipation of the short gravity waves; F is a filter function to restrict a region in the k-space where the short gravity waves lose energy through the nonlinear generation of the parasitic capillaries. This function should be close to one in the range $\sim 60\ \text{rad/m} < K < 1/2(g/\gamma)^{1/2}$, and falling rapidly outside this range. We specify a mapping of this function into the capillary interval as

$$F(k/k_c) = \exp\left(-4\left(\frac{k_c}{k}\right)^4\right) \tag{4-65}$$

for $k < 2000$ rad/m, and zero for $k > 2000$ rad/m. The solution of equation (4-64) is:

$$B(k,\phi) = \frac{1}{2}\alpha_{cg}\left[\beta_v + |\beta_v|\left(1 + 4\frac{\tilde{D}(K,\phi)\ F(k/k_c)}{\alpha_{cg}\beta_v^2}\right)^{1/2}\right] \tag{4-66}$$

where $\tilde{D} = K^{7/2}g^{-3/2}D$ is the dimensionless dissipation spectrum.

4.4.8 CAPILLARY WAVE SPECTRUM.

The energy input from the wind does not play a significant role in the balance of pure capillary waves, say at $k > 2k_c$. In this range the viscous dissipation balances the cascade

transfer of energy from the short gravity waves, which is proportional to the energy input from the wind:

$$D(K,\phi) \sim \beta_v g^{-3/2} K^{-7/2} B(K,\phi). \tag{4-67}$$

Substituting (4-67) into (4-66), and accounting for (4-45) the relation between the saturation spectra of the capillary $B(k, \phi)$ and the short gravity waves $B(K,\phi)$ *at* $k>2k_c$ follows

$$B(k,\phi) \sim (1-\alpha_c) u_*^2 \upsilon^{-1} \gamma^{-1/2} k^{-3/2} B(K,\phi) \cos^2(\phi). \tag{4-68}$$

From (4-68) immediately follows that the wind dependence of the CWs spectrum is at least quadratic. The saturation spectrum decreases with the increase of the wavenumber, and the angular spreading of the CWs spectrum is more narrow than the SGWs one.

At moderate winds the upwind directional curvature spectrum of the short gravity waves is B(K,0) ~ (u*/c) (Toba 1973), hence the spectrum of the capillary waves (4-68) takes the form:

$$B(k,0) \sim \frac{m_\beta}{4}(1-\alpha_c)\, u_*^3\, \nu^{-1}\gamma^{-1} k^{-2}. \tag{4-69}$$

The wind dependence of the model spectrum (4-69) is close to that observed experimentally by Jähne and Riemer (1990) in the capillary interval. The "-2" wavenumber power law for the curvature spectrum is consistent both with measurements of Jähne and Riemer (1990) and Zhang (1995).

4.4.9 GENERALIZED SHORT WAVE SPECTRUM

To obtain the generalised model of short wave spectrum the short gravity wave spectrum (4-63) is patched to the capillary-gravity spectrum (4-66) by specifying parameters α and n in the form:

$$\ln(\alpha) = (\ln(\alpha_{cg}) - \ln(\alpha_g))\,\varphi(k/k_c) + \ln(\alpha_g), \tag{4-70}$$

and

$$n^{-1} = \frac{1}{2}(\varphi(k/k_c) + 1), \tag{4-71}$$

where

$$\varphi(k/k_c) = \min[(k/k_c)^\mu, 1] \tag{4-72}$$

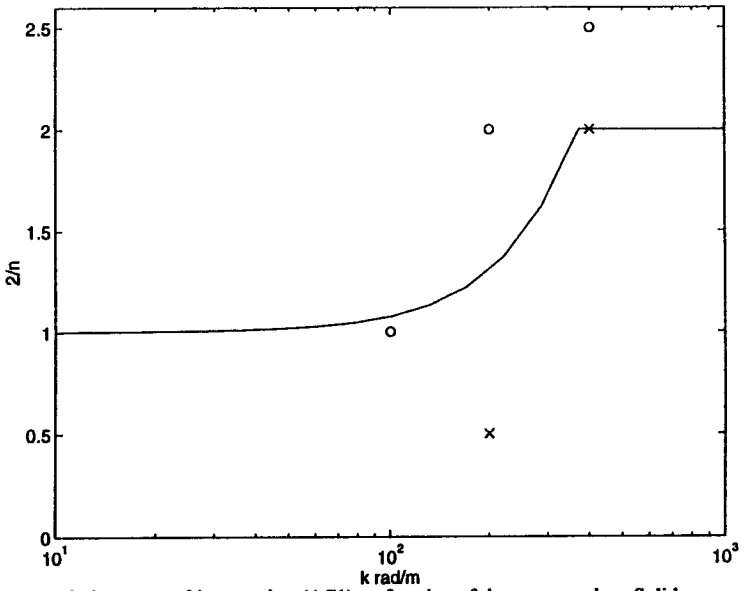

Figure 4.4 Wind exponent $2/n$, equation (4-71) as function of the wavenumber. Solid curve – model results; circles - measurements of Jähne and Riemer, (1990); crosses – measurements of Hara et al., (1997); value of Toba (1973) corresponds to 1.

Formally, function $\varphi(k/k_c)$ in (4-70) and (4-71) provides the patching. Its physical sense is that $\varphi(k/k_c)$ describes the transition between the regimes of energy losses dominated by wave breaking, emissions of parasitic capillary, and then by resonant 3-waves interactions. Parameter μ in (4-72) is defined by the comparison of the model wind exponent $p = 2/n$ with measurements of Jähne and Riemer (1990), Hara et al. (1997), and Toba (1973), shown in Figure 4.4. The solid curve fitted in measurements is the model wind exponent with μ=2.

To complete the model, the last two constants α_g and α_{cg} are to be defined. The former constant provides patching of the short gravity wave spectrum with the energy containing part of the Donelan et al. (1985) spectrum with correction of Elfouhaily et al. (1997). For a fully developed sea this constant is $\alpha_g = 8.2\,10^{-3}$. The latter constant α_{cg} is defined in Section 5.1.1 after comparisons the model results to measurements (Jähne, Riemer 1990; Hara et al. 1997) of the saturation spectrum at k ~200 rad/m and 400 rad/m. It will be shown that the fitting of the model to measurements gives $\alpha_{cg} = 7.1\,10^{-2}$.

Finally the generalized model of the short wind wave saturation spectrum in the range $k > k_r$ has the following form:

$$B(k,\phi) = \alpha\left\{\frac{1}{2}\left[\beta_v(k,\phi) + \left(B_v^2(k,\phi) + 4\alpha^{-1}\beta_v(K,\phi)B(K,\phi)F(k/k_c)\right)^{1/2}\right]\right\}^{1/n} \tag{4-73}$$

where k_r ~$10k_p$ is the lowest wavenumber restricting the applicability of the short wave spectrum model, and k_p is the peak wave number.

4.4.10 THE LONG GRAVITY WAVE SPECTRUM

Energy containing long waves in the peak of the wave spectrum with $k < k_r$ support a part (~10%-20%) of the momentum flux to the sea surface (Makin, Kudryavtsev 1997) and influence the balance of the short wind waves. A long wave spectrum is thus should be added to the described model of the short wave spectrum. For that the long wave spectrum model of Donelan et al. (1985) with correction of Elfouhaily et al. (1997) is chosen.

The long wave curvature spectrum B_l is

$$B_l(k,\phi) = \frac{1}{2}\alpha_p \frac{c_p}{c} F_p J_p f_{k,\phi} \tag{4-74}$$

where

$$\alpha_p = 0.006\Omega^{0.5} \tag{4-75}$$

is the equilibrium range parameter, dependent on the inverse wave-age parameter $\Omega = U_{10}/c_p$. The side-effect function F_p is introduced by Elfouhaily et al. (1997) as

$$F_p = \exp\left\{-\frac{\Omega}{\sqrt{10}}\left(\sqrt{\frac{k}{k_p}} - 1\right)\right\}. \tag{4-76}$$

J_p is the JONSWAP peak enhancement function.

$$J_p = \gamma^{\Gamma}\exp\left\{-\frac{5}{4}\left(\frac{k_p^{\,2}}{k}\right)\right\}, \tag{4-77}$$

$$\gamma = 1.7 + 6\log(\Omega),$$
$$\Gamma = \exp(-(\sqrt{k/k_p} - 1)^2/2\sigma^2), \tag{4-78}$$
$$\sigma = 0.08(1 + 4\Omega^{-3}).$$

The angular spreading function $f_{k,\phi}$ according to Donelan and Pierson (1987) is

$$f_{k,\phi} = \frac{1}{2}h(k)\cosh^{-2}(h\phi) \tag{4-79}$$

where $h(k)$ is an empirical function defined in Donelan and Pierson (1987).

The long wave spectrum (4-74) is overlapped with the short wave spectrum (4-73).The side-effect function F_p provides the smooth matching of the spectra around the wave number k_r.

Equations (4-39), (4-40), (4-73), and (4-74) describe the coupled evolution between wind waves and the atmospheric boundary layer.

4.5 Results

4.5.1 PARAMETERS OF THE SEA SURFACE

As it was shown in early studies (Janssen 1989; Makin et al. 1995; Makin 1997; Makin, Kudryavtsev 1997) the form of the wave spectrum in the range of short waves forms a significant part of the surface momentum to waves, and in fact, defines the sea drag for moderate to strong winds. In a physical model of the short waves, the form of the spectrum results from the counteraction of many physical mechanisms in a coupled system sea surface-atmosphere. To have the right estimates of the sea drag (and the other parameters of the atmosphere), the correct description of the sea surface parameters, both spectral and integral, should be ensured.

4.5.2 SPECTRAL CHARACTERISTICS

Figure 4.5 and Figure 4.6 show the proposed saturation spectrum and laboratory measurements of the upwind $B(k,0)$ and the omni-directional $B(k)$ saturation spectra at wavelengths λ=0.008 m (k = 785 rad/m), λ=0.016 m (k = 393 rad/m), λ=0.031 m (k =203 rad/m), and λ=0.063 m (k = 100 rad/m), reported by Jähne and Riemer (1990) and Hara et al. (1997). The measured values of the saturation level at λ=0.016 m and λ =0.031 m were used to adjust α_{cg} to the value $7.1\,10^{-2}$. Overall good agreements are then obtained for λ=0.008 m, a wave component which corresponds to the parasitic capillary range: the capillary wave spectrum resulting from (4-73) at $k > 2k_c$, does not require further adjustments and directly results from the short gravity wave spectrum. This may justify that the generation of the parasitic capillaries indeed plays the dominant role in the balance equation of the capillary waves.

In the gravity range, λ=0.063 m, the data of Jähne and Riemer (1990) are only available. The comparison is reasonable for the lowest values of the friction velocity. At larger values the measured values of the saturation level exceed the model ones. However that was already the case for λ=0.031 m, where the model curve was fitted to lie between the measurements of Jähne and Riemer (1990) and Hara et al. (1997).

The upwind and omni-directional wave spectra at various wind speeds are shown in Figure 4.6. At low winds there is a spectral gap in the vicinity of $k \sim (g/\gamma)^{1/2}$, which fills up when the wind speed increases. Such a peculiarity in the spectral form was observed in the laboratory experiments of Cox (1958), and Zhang (1995). The origin of this spectral gap at low winds is caused by the viscous dissipation which increases towards the higher wave numbers and results in the decreasing of the saturation spectrum. The gap occurs at wave numbers up to $k \sim 2(g/\gamma)^{1/2}$. At higher wave numbers, the generation of parasitic capillaries takes place. A local spectral peak is formed in the vicinity of k=1000 rad/m and moves to k=700 rad/m with increasing wind speeds. In the capillary range the wavenumber power law for the saturation spectrum corresponds to -2. This is again consistent with Jähne and Riemer (1990), and Zhang (1995), though the model power law is slightly less than the observed one (-2 to -2.5).

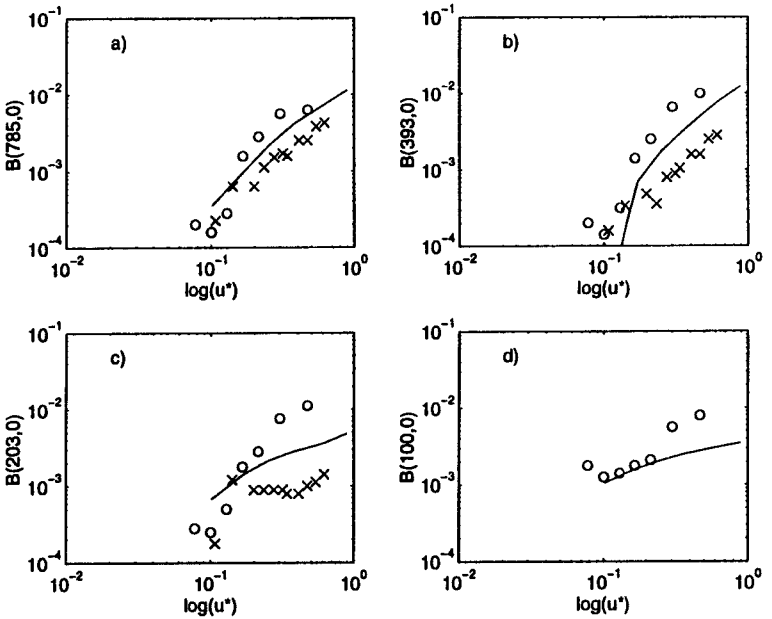

Figure 4.5 Up-cross section of the saturation spectrum $B(k,0)$ versus the friction velocity u_*. Solid line - model results; circles - measurements of Jähne and Riemer (1990); crosses - measurements of Hara et al. (1997).

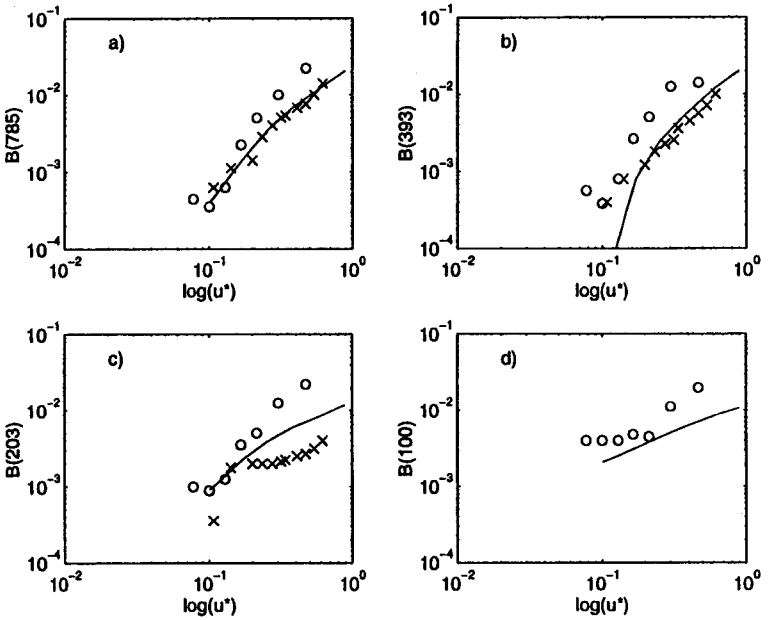

Figure 4.6 The same as in Figure 4.5 but for omni- directional saturation spectrum $B(k)$.

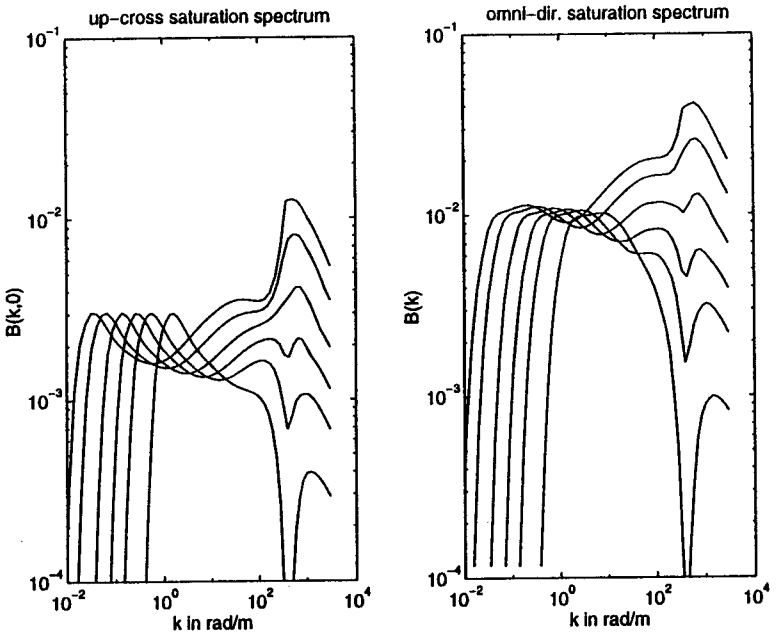

Figure 4.7 a) Up-cross section of the saturation spectrum $B(k,0)$ versus the wavenumber k for different wind speeds u_{10}. Curves from bottom to the top: 3 m/s, 5 m/s, 7 m/s, 10 m/s, 15 m/s, and 20 m/s. b) The same as in a) but for omni- directional saturation spectrum $B(k)$.

4.5.3 INTEGRAL CHARACTERISTICS OF THE SPECTRUM

Surface mean squared slope .The mean squared slope of the sea surface is mainly supported by the short wind waves, hence this integral parameter can be used to check the model consistency. The model estimates of the up-wind $<\zeta_x^2>$ and the cross-wind $<\zeta_y^2>$ mean squared slopes are:

$$<\zeta_x^2> = \int \cos^2(\phi)\, B(k,\phi)\, d\phi d(\ln(k)) \tag{4-80}$$

and

$$<\zeta_y^2> = \int \sin^2(\phi)\, B(k,\phi)\, d\phi d(\ln(k)). \tag{4-81}$$

The total mean squared slope (mss) ζ_0 is:

$$\zeta_0 = <\zeta_x^2> + <\zeta_y^2>, \tag{4-82}$$

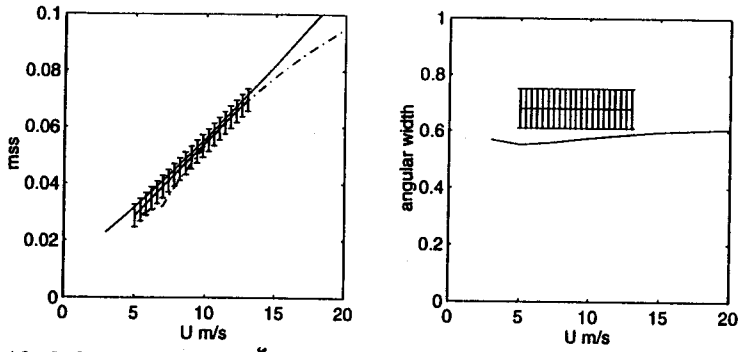

Figure 4.8 Left: mean square slope ζ_0 versus the wind speed u_{10}. Solid curve - model results, solid line with bars - regression line of Cox and Munk (1954), dashed-dotted – regression line of Wu (1990). Right: ratio $<\zeta_y^2>/<\zeta_x^2>$ versus the wind speed u_{10}. Solid curve - model results, solid line with bars - regression of Cox and Munk (1954).

Figure 4.8 gives model and measured (Cox, Munk 1954) inferred mean squared slopes as function of the wind speed (the reanalysis of Cox and Munk data done by Wu (1990) is also shown). Overall good agreements are obtained. The ratio $<\zeta_y^2>/<\zeta_x^2>$ is an integral measure of the spectrum angular anisotropy. This ratio versus the wind speed is given in Figure 4.8. The angular distribution widens with increasing wind speeds. It is mainly due to the spectral broadening in the capillary-gravity interval with increasing winds. Cox and Munk (1954) did not observe any systematic trend in $<\zeta_y^2>/<\zeta_x^2>$. Nevertheless, their reported averaged value 0.68 is only slightly exceeds the model estimate.

Skewness of the sea surface slopes In their experiment, Cox and Munk (1954) also reported skewness measurements of the surface slopes. It was defined by a shift from the specular direction of the brightest point in the sun glitter. Longuet-Higgins (1982) analyzed different mechanisms that could contribute to the skewness, and concluded that the most probable one is the modulation of the short wind waves by the longer ones. The simple sea surface model, adopted by Longuet-Higgins (1982), consists of the sum of a "long" wave and a "short" wave modulated by the "long" one:

$$\zeta_x = AK\sin\phi + [ak + \delta(ak)\cos(\phi-\gamma)]\sin\phi', \tag{4-83}$$

where ζ_x is the up-wind slope of the wave surface, AK and ak are the steepness of the "long" and the "short" wave respectively, ϕ and ϕ' are their phase functions; $\delta(ak)$ is the amplitude of the short wave steepness modulation, and γ is the phase of the modulation. Such a two-scale model gives

$$<\zeta_x^3> = \frac{3}{2}AK(ak\delta(ak))\sin\gamma \tag{4-84}$$

According to the present development, the parasitic capillaries are spread out on the forward face of short gravity waves, and attenuate due to the viscous dissipation. Hence, we can take $\sin\gamma = 1$ and $\delta(ak)=ak$. Since the wind input is negligible in generation of

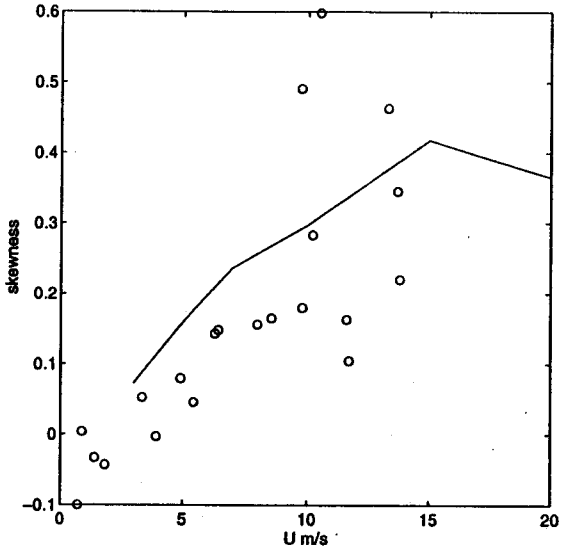

Figure 4.9 Skewness coefficient, equation (4-86), versus the wind speed u_{10}. Solid curve - model results, circles - analysis of Longuet-Higgins (1982) based on data of Cox and Munk (1954).

parasitic capillaries (see Section 4.3), the model skewness is defined as

$$<\zeta_x^3> = 3\sqrt{2}\left[\int_{k_1}^{k_c/2} B(k,\phi)\cos^2 d\phi d(\ln k)\right]^{1/2}\int_{k>2k_c} B(k,\phi)\cos^2\phi d\phi d(\ln k) \tag{4-85}$$

where $k_1=2\pi/0.15$ rad/m is the lowest wavenumber which restricts the interval of the short gravity waves generating the parasitic capillaries. The skewness coefficient

$$\lambda_3 = \frac{<\zeta_x^3>}{<\zeta_x^2>^{3/2}} \tag{4-86}$$

is shown in Figure 4.9. The values of λ as calculated by Longuet-Higgins (1982) from Cox and Munk's (1954) data are also presented. The model skewness values only related to parasitic capillaries are comparable with the observed ones and indicate the dominant influence of their generation on slope skewness measurements.

4.5.4 WHITECAP COVERAGE

Fraction of the sea surface covered by whitecaps dW which are generated by a narrow band of surface waves can be related to the number of breakers passing a given point per unit time $N(c,\phi)dcd\phi$

$$dW \sim \frac{2\pi}{\omega} N(\overrightarrow{c})\, dc d\phi \qquad (4\text{-}87)$$

The constant of proportionality in (4-87) relates to the ratio of the individual white caps scale to the wave length. As the breakers of different scale are similar, this constant should be the same for all breaking waves.

Integrating (4-87) and taking into account relation (4-57) the total fraction of the whitecaps coverage is expressed directly via the saturation wave spectrum B

$$W \sim \pi \int_0^{k_b} \left(\frac{B(k,\phi)}{\alpha_g} \right)^{n_g+1} d(\ln k)\, d\phi \qquad (4\text{-}88)$$

The upper limit of integration k_b corresponds to the wave length of 10-15 centimeters, as for shorter waves the losses of energy is mainly due to the generation of the parasitic capillary waves and not due to breaking.

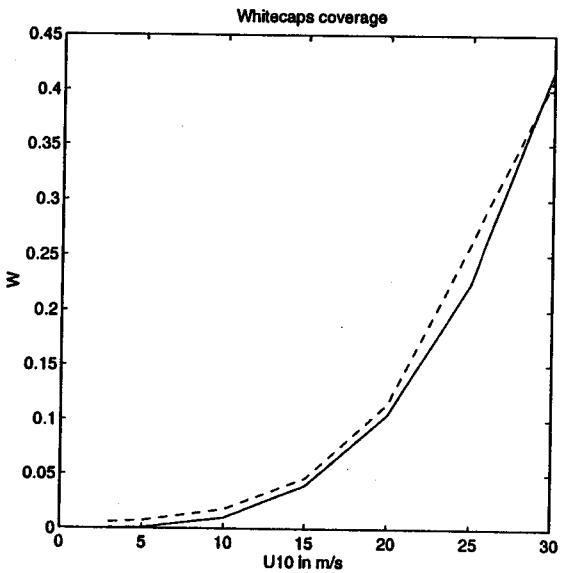

Figure 4.10 Whitecap coverage versus the wind speed u_{10}. Solid curve - model results, equation (4-88), dashed - empirical relation of Monahan et al. 1986), equation (4-10).

The instantaneous fraction of the sea surface covered by whitecaps as directly calculated from the model saturation spectrum according to (4-88) (with a proportionality constant equal to 1) is compared with an empirical relation (4-10) by Monahan et al. (1986) in Figure 4.10. A fair agreement is found up to the wind speed of 30 m/s. In Section 6 the relation (4-88) for the whitecap coverage will be used to calculate production of spray droplets by breaking waves.

4.5.5 PARAMETERS OF THE ATMOSPHERE

4.5.5.1 The sea drag and the coupling parameter

The model coupling the sea surface and the atmosphere must in the first place reproduce the known wind speed dependency of the drag coefficient C_D. In Figure 4.11 - a the model results are shown together with parameterizations of the drag coefficient obtained in the open ocean (Anderson 1993; Large, Pond 1982; Smith 1980; Donelan, Pierson 1987), see Table 4.1. Considering a typical error in stress measurements of about 15%-20% (Donelan 1990), the model results compare well with observations.

Table 4.1 Regressions of drag coefficient on wind speed

Authors	Regression 10^3 CD	Wind speed range
Donelan and Pierson (1987)	$0.96 + 0.041\ U_{10}$	$4 < U_{10} < 16$
Large and Pond (1982)	$0.49 + 0.065\ U_{10}$	$10 < U_{10} < 20$
	0.14 ± 0.20	$5 < U_{10} < 10$
Smith (1980)	$0.61 + 0.063\ U_{10}$	$6 < U_{10} < 22$
Anderson (1993)	$0.40 + 0.079\ U_{10}$	$4.5 < U_{10} < 21$
	$0.59 + 0.065\ U_{10}$	$U_{10} > 10$

It is emphasize, that the drag of the sea surface is calculated from dynamically coupled system wind waves-atmosphere. Few basic assumptions concerning the local properties of the sea surface, and momentum exchange at the sea surface allows to obtain independently the main parameter of the atmosphere - the drag coefficient. The sea roughness results in this approach from the dynamical coupling of waves with the atmosphere.

The sea surface drag is supported by the viscous stress and the wave-induced momentum flux to waves. The coupling parameter α_c, the principle parameter characterizing the wind over waves coupling, equation (4-40), is shown in figure 4.11b for a fully developed sea. For low wind speeds $u_{10} < 5$ m/s, the stress at the surface is dominated by the viscous drag, so most of momentum is transferred directly from the air flow to the water flow. This is in agreement with observations, that the sea surface is aerodynamically smooth for wind below 2 - 3 m/s (Geernaert 1990). Analysis of the field experiment of Snyder et al. (1981) by Harris et al. (1996) suggests that the water surface is more likely to be transitional or even smooth, than rough for the conditions of the experiment (the range of wind speeds is 2 - 7 m/s). Results, presented in Figure 4.11b support this conclusion, that for light winds, a significant part of momentum is transferred by viscous stress. The recent direct laboratory measurements of the surface fluxes (Banner, Pierson 1996) have shown, that for the wind speed of 7 m/s the coupling parameter is about 0.38, while for the wind speed 13 m/s it should be about or less than 0.67, in excellent agreement with the present model results, see Figure 4.11b. For the wind speeds of about 15 m/s and higher, most of the stress goes through waves and sea becomes aerodynamically rough.

4.5.5.2 Wind-induced stress at the surface

To assess which waves contribute most to the wave-induced stress at the surface the surface flux spectrum $T(k)$ (equation (4-25)) and the cumulative spectrum Cu(k) are shown in Figure 4.12 for different wind speeds. The cumulative spectrum is

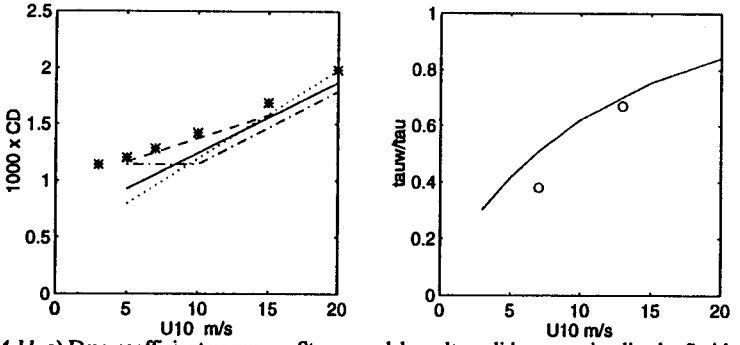

Figure 4.11 a) Drag coefficient versus u_{10}. Stars - model results; solid - regression line by Smith (1980); dashed-dotted - regression line by Large and Pond (1982); dashed – regression line by Donelan and Pierson (1987): dotted - regression line by Anderson (1993). b) Coupling parameter $\tau^w(0)/u_*^2$, solid line - model results; circles - experiment of Banner and Peirson (1996).

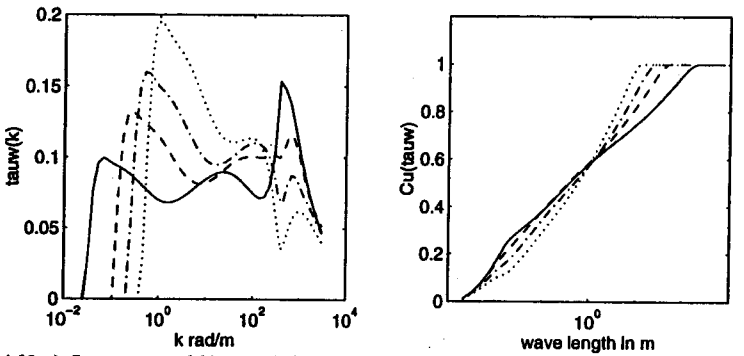

Figure 4.12 a) Spectrum, and b) cumulative spectrum of the wave-induced stress at the sea surface; wind speed u_{10}= 20 m/s - solid, 10 m/s - dashed, 7 m/s - dashed-dotted, 5 m/s – dotted.

$$Cu(k) = \frac{1}{\tau_0^w}\int_k^\infty T(k)\, d(\ln k)\,. \qquad (4\text{-}89)$$

The latter is shown as a function of the wave length $\lambda=2\pi/k$ and shows an increase in the wave-induced stress as more an more longer waves are taken into account in the integral (4-89). The wavenumber of the peak of the spectrum is 0.068 rad/m which corresponds to a wave length of 93 m.

Waves in the spectral peak support only a small part of the total momentum flux to the sea surface. Most of the momentum is supported by relatively short waves. At low winds almost all of the form drag is supported by waves shorter than 10 m, and 50% of the form drag is supported by waves shorter that 0.5 m. About 5% of this is supported by capillary waves with lengths $\lambda<$ 0.017 m. So, at low wind the decimeter and meter waves play the dominant role in wind over waves coupling.

With increasing wind the role of short gravity and capillary- gravity waves in wind over waves coupling becomes more important. At high winds (U_{10}= 20 m/s) a local spectral maximum develops in the vicinity of k=700-800 rad/m, and the short waves in the range of the wave length 0.001 - 0.1 m contribute about 40% to the form drag. They play the dominant role in extracting momentum and are strongly coupled with the atmosphere. It is interesting to note that for all wind speeds about 50% of the wave-induced stress is supported by waves shorter than 1 meter, though the spectral distribution of this flux is rather different for low and high wind speeds. Waves longer than 10 m extract about 20% of the form drag and should thus be accounted for in the description of wind wave spectrum.

The above analysis shows that most of the momentum to waves is transferred to centimetre to metre waves, so that the sea drag depends crucially on the form of the wave spectrum in the corresponding wavenumber range. It becomes clear that the sea drag relates directly to the spectral density of short waves. If a large scale physical process influence the spectral density of these waves, that will be immediately reflected in the increase/decrease of the drag coefficient (friction velocity) above the sea.

4.5.5.3 Wave age dependence of the sea drag

In the last decade a strong attention is drawn to the problem of the wave age dependence of the drag coefficient, both from theoretical and experimental sides. As far no consensus is reached, and the points of view range enormously.

In the recent review on the problem (Komen et al. 1998) it is mentioned that the correct parameterization of the drag dependence on the sea state (and the wind) is of considerable importance for the formulation of the scaling laws of fetch- and duration-limited wave growth, for weather forecasting and climate modelling (Janssen, 1994; Janssen, Viterbo 1995), implications for storm surge modelling (Mastenbroek et al. 1993), remote sensing applications, and many other meteorological and oceanological applications.

Original data analysis of the Humidity Exchange over the Sea Main Experiment (HEXMAS), as reported by Smith et al. (1992), compilation of data, obtained at different sites near the shore and in the open ocean, reported by Donelan et al. (1993) seem to support the point of view that the sea drag does depend on the wave age parameter, increasing with increase of the inverse wave age parameter $\Omega=u_{10}/c_p$, meaning that the drag for old seas ($\Omega\leq 1$) is smaller than for young seas ($\Omega>$ 1) at the same wind speed.

Open sea measurements by Yelland and Taylor (1996) in the sufficient range of the wave age parameter however does not offer that possibility, the drag is found to be fairy constant for the wave ages under consideration. Reanalysis of HEXMAS data by Janssen (1997) and Oost (1998) reveal sufficient drawbacks of the original analysis. The wave age dependence found in Smith et al. (1992) is hinged on only few data points at high wind speed when the waves already feel the finite depth at the site of measurements. Moreover the measurements could be contaminated by strong currents typical for the site (Komen et al. 1998). The conclusion by Janssen (1997) was that the HEXMAS data does not offer the prove for the wave age dependence of the sea drag as the effect of sea-state on wind stress is much smaller that the experimental noise level.

Toba et al. (1990), Jones and Toba (1995) suggest quite an opposite trend in wave age dependence of the sea drag arguing that the drag is larger for old seas that for young ones.

However near-shore measurements normally give larger values of the sea drag compared to the open sea measurements. The question whether the near-shore measurements are representative for conditions in the open sea and can be analysed together is risen in Makin et al. (1995), and Komen et al. (1998). The finite depth effects could actually define the large variability of the drag. Geernaert (1990) has shown that the drag clearly could be stratified by the depth at site of measurements. Other local effects as currents, effects of upwind roughness over the land, slicks can matter.

We also mention the problem of huge scatter in the dimensionless Charnock parameter $z_0^* = z_0 g/u_*^2$ associated with errors in the measurements of the friction velocity (Komen et al. 1998).

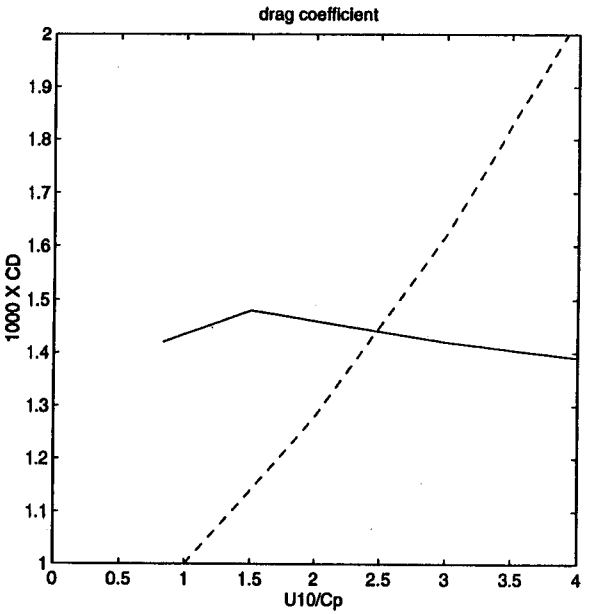

Figure 4.13 Wave age dependence of the drag coefficient. Solid line - model spectrum, dashed-dotted – JONSWAP spectrum. u_{10}= 10 m/s.

The wind over waves coupling theory allows a different approach to the problem. As is shown is the previous section the most of the momentum is transferred to centimetre to metre waves, so that the sea drag depends crucially on the form of the wave spectrum in the corresponding wavenumber range. The wave age dependence of the sea drag is thus determined by the form of this high wavenumber spectrum tail. If the tail is wave age independent, the sea drag appears to be virtually independent of wave age. If the tail depends on wave age, the drag would also depend on. This fact is illustrated in Figure 4.13 where the sea drag is calculated with the JONSWAP spectrum which is proportional to $S(k) \sim (u_{10}/c_p)^{3/2}$ in the full wavenumber range. According to such dependence the tail of JONSWAP spectrum moves up for younger seas (inverse wave age parameter u_{10}/c_p is increasing) and down for developed seas. That immediately introduce a significant wave age dependence of the sea drag. Calculations performed with the model spectrum show no wave age dependence of the sea drag as the high wavenumber tail (4-73) has no dependence on wave age. As far there is no direct experimental evidence that waves in the high wavenumber range depend on wave age.

The near shore measurements on limited depths which usually show higher values of the drag coefficient for the same wind speed, compared to the open ocean measurements, however seems to testify that the high wavenumber tail of wave spectra in near shore conditions differs from one in the open ocean. The physical mechanisms responsible for this difference are not clear. There could also remain a possibility that intensified breaking in the shallow waters is responsible for the increased sea drag.

4.6 Heat fluxes in presence of spray

In the literature it is argued that for wind speeds above about 15 m s^{-1} the effect of the sea spray evaporation becomes important and influence sensible heat and humidity fluxes. Andreas (1992) has suggested a theory and found for a wind speed of U_{10}= 20 m s^{-1} a droplet mediated latent heat flux of 45% of a direct latent heat flux. Fairall et al. (1994) used a simplified and generalised derivative of an approach developed by Andreas (1992) and have shown that the contributions of oceanic spray to air-sea fluxes become comparable to direct turbulent fluxes at wind speeds above about 20 m s^{-1}. On the contrary, Hasse (1992), using some general theoretical arguments, argued that there could be hardly any effect of spray evaporation on heat fluxes (perhaps, except for hurricane wind strength).

The hostile environment of rough seas makes direct measurements of sensible and humidity fluxes over the open sea extremely difficult, and only few measurements of those exists. The main goal of the Humidity Exchange over the Sea Main Experiment (HEXMAX) program (DeCosmo et al. 1996; Katsaros et al. 1987, 1994; Smith et al. 1996) was to find accurate empirical heat and moisture flux parameterization formulas for high wind conditions over the sea. It had been postulated that breaking waves and sea spray, which dominate the air-sea interface at high wind speeds, would significantly affect the air-sea heat and moisture exchange for wind speeds above 15 m s^{-1}. The outcome of the experiment was rather disappointing: no significant variation with wind speed has been found for wind speeds up to 18 m s^{-1} for humidity exchange coefficient and up to 23 m s^{-1} for sensible heat exchange coefficient. Large and Pond (1982), Anderson (1993) reported measurements of sensible heat flux up to 23 m s^{-1} under unstable conditions. No significant variations with wind speed was found either. As far, there is no direct experimental evidence that the evaporation of droplets plays a significant role in heat and moisture transfers. Measurements beyond a wind speed of about 23 m s^{-1} are needed to settle the issue.

In the wind over waves coupled model the impact of the spray mediated flux on sensible heat and humidity exchange coefficients can be easily assessed (see, also Makin 1998). In choosing an empirical droplet concentration function, which determines the magnitude of the spray mediated flux, the following requirement was imposed. The calculated sensible heat exchange coefficient should agree with measurements, thus no significant variations due to the impact of sea spray should be obtained for wind speeds below 18 m s^{-1}. The exchange coefficients are then evaluated for the wind speeds up to 30 m s^{-1} and their windspeed dependence in presence of sea spray is assessed.

4.7 Balance equations for sensible heat and humidity

The spatially averaged (4-5) balance equations of sensible heat and humidity above waves in the stationary WBL read

$$-\frac{\partial \overline{\theta' w'}}{\partial z} + \varepsilon(z) = 0, \tag{4-90}$$

$$-\frac{\partial \overline{q' w'}}{\partial z} + E_v(z) = 0. \tag{4-91}$$

In equations (4-90)-(4-91), θ is the mean potential temperature in K°, q is the mean specific humidity in $kg_w\ kg_a^{-1}$. The $\tau_\theta^t = -\overline{\theta' w'}, \tau_q^t = -\overline{q' w'}$ are the mean turbulent kinematic fluxes of sensible heat and humidity, and E_v and E are the source (sink) functions resulting from the evaporation of spray. The function E relates to the evaporation function E_v

$$E = -\frac{L_v}{C_p} E_v \tag{4-92}$$

where L_v is the latent heat of vaporization of water, $C_p = C_{pd}(1+0.84q)$ is the specific heat of moist air at constant pressure, and C_{pd} is that of the dry air. The dimension of E_v is $kg_w\ kg_a^{-1}\ s^{-1}$.

The evaporation of droplets increases humidity of the air and thus $E_v > 0$, and decrease the air temperature.

It is convenient to rewrite equations (4-90) and (4-91) in the flux form

$$-\frac{\partial \overline{\theta' w'}}{\partial z} + \frac{\partial \tau_\theta^s}{\partial z} = 0, \tag{4-93}$$

$$-\frac{\partial \overline{q' w'}}{\partial z} + \frac{\partial \tau_q^s}{\partial z} = 0, \tag{4-94}$$

where

$$\tau_\theta^s(z) = -\int_z^\infty E(z)\, dz, \tag{4-95}$$

$$\tau_q^s(z) = -\int_z^\infty E_v(z)\, dz \tag{4-96}$$

are the spray mediated fluxes of sensible heat, and humidity.

In the stationary WBL the total flux of sensible heat and humidity is constant over height. The wave-induced fluxes τ_θ^s and τ_q^s are negligible at the top of the WBL z=h, which is secured by the exponential decay of the droplet concentration, see equation (4-115). Thus constants are defined by the turbulent fluxes at the top of the WBL, i.e., $-\overline{\theta' w'}_h = \theta_* u_*$, and $-\overline{q' w'}_h = q_* u_*$. The total fluxes are

$$\tau_\theta = \tau_\theta^t(z) + \tau_\theta^s(z) = \text{const} = \theta_* u_* = -\overline{\theta' w'}_h, \tag{4-97}$$

$$\tau_q = \tau_q^t(z) + \tau_q^s(z) = \text{const} = q_* u_* = -\overline{q' w'}_h. \tag{4-98}$$

In (4-97)-(4-98) θ_* and q_* are the temperature and humidity turbulent scales.

4.7.1 TURBULENT FLUX

Following the local closure, eddy-viscosity K theory, the turbulent flux of sensible heat is written as

$$\tau_\theta^t(z) = -\overline{\theta' w'} = K_\theta \frac{\partial \theta}{\partial z}, \tag{4-99}$$

and turbulent flux of humidity is

$$\tau_q^t(z) = -\overline{q' w'} = K_q \frac{\partial q}{\partial z}. \tag{4-100}$$

The turbulent diffusivity of heat K_θ and humidity K_q depends on the state of turbulence and is closely related to the eddy-viscosity K via the turbulent Prandtl and Schmidt numbers:

$$K_\theta = \frac{K}{\mathrm{Pr}_t}, \tag{4-101}$$

$$K_q = \frac{K}{\mathrm{Sc}_t}. \tag{4-102}$$

As is mentioned, e.g., by Donelan (1990) and Rodi (1984), the buoyancy forces produced by temperature and humidity differences affect the values of the turbulent Prandtl and Schmidt numbers. Empirical data compiled, e.g., by Zilitinkevich (1970, Figure 1.22), show that the Prandtl number for stable stratification is larger than that for unstable stratification. Based on these data, the value of $\mathrm{Pr}_t = 0.9$, for unstable and the value of $\mathrm{Pr}_t = 1.25$ for stable stratification is adopted here. Further, there is commonly assumed that for the atmospheric flows $\mathrm{Sc}_t = \mathrm{Pr}_t$ (Large, Pond 1982; Donelan 1990).

4.7.1.1 Stratification effects

The easiest way to account for stratification effects on the structure of the WBL is to introduce empirical universal flux-profile functions (e.g. Donelan 1990). We simply redefine the mixing length l in (4-22) as

$$l = \kappa z\, \Phi^{-1}(z/L) \tag{4-103}$$

where L is Monin-Obukhov length scale calculated from the temperature and humidity turbulent scales θ_* and q_*.

$$L = \frac{u_*^2\, \theta}{\kappa g\, u_* (\theta_* + 0.61 q_* \theta)}. \tag{4-104}$$

The turbulent diffusivity coefficients of heat and humidity take the form

$$K_{\theta,q} = K \frac{\Phi}{\Phi_{\theta,q}} \tag{4-105}$$

where the flux-profile functions are (Dyer 1974; Stull 1991)

$$\begin{aligned} &\Phi(z/L) = (1-16z/L)^{-1/4} \quad z/L < 0, \\ &\Phi(z/L) = 1+5z/L \qquad\quad z/L > 0 \end{aligned} \tag{4-106}$$

$$\begin{aligned} &\Phi_{\theta,q}(z/L) = \Phi_{\theta,q}(0)\,(1-16z/L)^{-1/2} \quad z/L < 0 \\ &\Phi_{\theta,q}(z/L) = \Phi_{\theta,q}(0)\,(1+5z/L) \qquad\quad z/L < 0 \end{aligned} \tag{4-107}$$

and $\Phi_{\theta,q}(0) = \mathrm{Pr}_t$.

4.7.2 EVAPORATION FUNCTION

After Pruppacher and Klett (1978) (see also Fairall et al. 1994), the evaporation function $E_v(z)$ can be calculated from the known distribution of the droplet concentration $n(r,z)$. The rate of loss of mass by evaporation $\dot{m}$ by a single droplet of radius r (in m) is

$$\dot{m} = -4\pi F_p D_v \rho_a r (q_s - q) \tag{4-108}$$

where q is the ambient specific humidity, and q_s is the saturation specific humidity at the droplet temperature. The diffusivity of water vapor D_v (Pruppacher, Klett 1978) is

$$D_v = 0.21 \times 10^{-4} \left(\frac{T}{T_0}\right)^{1.94} \left(\frac{p_0}{p}\right) \tag{4-109}$$

with $T_0 = 273°\mathrm{K}$, $p_0 = 101.3\,\mathrm{kPa}$. Dimension of D_v is in $\mathrm{m^2\ s^{-1}}$. The value of pressure at the sea level for a standard atmosphere is used here, i.e., $p=p_0$. The difference between the absolute temperature T and the potential temperature θ in the surface boundary layer can be neglected.

The droplet ventilation (Pruppacher, Klett 1978; Fairall et al. 1994) is

$$F_p = 1 + 0.25 \left(\frac{2V_f r}{\nu}\right)^{0.5} \tag{4-110}$$

where $V_f = 8000\, r$ is the terminal fall velocity.

To account for the fact that droplets are maintained at the wet bulb temperature rather than the air temperature, we follow Fairall et al. (1994) and write

$$q_s - q = \gamma \left[q_s(\theta) - q\right] \tag{4-111}$$

where γ is given by

$$\gamma = \left[1 + \frac{\varepsilon L_v^2}{R\, C_p T^2} q_s(\theta)\right]^{-1}, \tag{4-112}$$

ε is the ratio of gas constants for air and water vapor, and R is the gas constant for air.

It is convenient to express the saturation specific humidity q_s as a function of temperature. According to Stull (1991)

$$q_s = \varepsilon \frac{0.6112}{p_0} \exp\left[\frac{17.67\,(T-273.16)}{T-29.66}\right] \tag{4-113}$$

The total loss rate of liquid water by evaporation at some level z is obtained by integrating equation (4-108) over the number concentration of droplets, $n(r,z)$:

$$-E_v(z) = \int \dot{m} n(r,z)\, dr. \tag{4-114}$$

As $q_s(\theta_z) - q(\theta_z) > 0$, $\dot{m} < 0$, and the evaporation function $E_v(z)$ is positively defined.

The vertical profiles of temperature θ_z and humidity q_z can be obtained by integrating equations (4-97)- (4-98).

4.7.2.1 Droplet Concentration

To evaluate the evaporation function E_v, the vertical distribution of the droplet concentration $n(r,z)$ should be known. The approach by Smith et al. (1993) is followed here, and it is assumed that the average droplet concentration, at a given wind speed, represents the equilibrium distribution. That is, the loss of droplets due to turbulent deposition and gravitational sedimentation is balanced by the new droplet production.

To evaluate the average droplet concentration $n(r,z)$ above the waves, a simple model based on general experimental knowledge is used. The model captures the main known features of the droplet distribution in the WBL, namely, the proportionality of the droplet concentration to the whitecap coverage of the sea surface, and a fast decay of

droplet concentration with height above the waves (Wu 1990). The sea spray generated by bursting bubbles, produced by the air entrainment by breaking waves, is discussed here. Two types of droplets are produced by bursting bubbles. Film droplets are produced through the fragmentation of bubble caps, and jet droplets are produced through the breakup of a water jet formed by the collapse of bubble cavity (Wu, 1992). As was shown by Wu (1989), the sea spray under various wind conditions consists mainly of jet droplets, as the dominance of jet droplets over film droplets is just too overwhelming. The contribution of film droplets to the average concentration thus can be neglected.

Field measurements (Preobrazhenskii 1973), laboratory measurements, and their numerical simulation (Edson, Fairall 1994; Edson et al. 1996) show that the concentration of jet droplets decays exponentially with height

$$n(r,z) = N_0 \exp(-z/z_e) \tag{4-115}$$

where z_e is a characteristic decay length and N_0 is the surface droplet concentration. It is usually assumed that the decay length is proportional to the significant wave height $z_e = c_e H_s$ (Andreas 1992; Andreas et al. 1995; Fairall et al. 1994; Edson et al. 1996), which can be directly calculated from the directional wave spectra (4-73) and (4-74)

$$H_s = 4\sqrt{\overline{\eta^2}}. \tag{4-116}$$

The mean squared elevation is defined by

$$\overline{\eta^2} = \int_0^\infty \int_{-\pi}^{\pi} S(k,\phi)\, k\, dk\, d\phi, \tag{4-117}$$

and the proportionality coefficient $c_e = 0.25$, as discussed in Makin (1998).

Wu (1992) suggested calculating the concentration of jet droplets from the bubble population at the sea surface which is proportional to the probability density of bubbles p and the total bubble concentration at the surface N_b. Relating the bubble diameter to the droplet radius a probability density $p(r)$ (Wu 1992) is

$$\begin{aligned} &p(r) = 0 && r \le 4.18\mu m \\ &p(r) = 0.015 && 4.18\mu m < r < 6.25\mu m \\ &p(r) = 23\, r^{-4} && r \ge 6.25\mu m \end{aligned} \tag{4-118}$$

The total bubble concentration at the surface is directly related to the whitecap coverage function W. Comparing the empirical function $N_b = 57\, U^{3.5}$ given by Wu (1988) with empirical function $W(u_{10})$ given by Monahan et al. (1986), relation (4-10), the obvious relation connecting the bubble production to the whitecap coverage is found

$$N_b = 20 \times 10^6 W. \tag{4-119}$$

The production of jet droplets by bubbles is expressed by Wu (1992)

$$n_j(r) = 7\exp(-16r/3000), \tag{4-120}$$

and the concentration of droplets N_0 is thus

$$N_0 = N_b p(r)\, n_j(r). \tag{4-121}$$

The vertical droplet concentration $n(r,z)$, equation (4-115), and the evaporation function $E_v(z)$, equation (4-114), can be finally calculated. The range of the jet droplets contributing mainly to the total droplet concentration is $5\,\mu m < r < 100\,\mu m$ (Andreas 1994; Edson, Fairall 1994; Fairall et al. 1994).

As is shown in Section 4.5.4 the whitecap coverage function W can be calculated from the density of frequency of wave breaking events $N(c,\phi)$, which in turn is related to the form of the wave spectrum via (4-57). Using equation (4-88) the concentration of droplets is related to the form of the wave spectrum, which is a solution of the model of a coupled system waves-atmosphere.

4.7.3 SENSIBLE HEAT AND HUMIDITY EXCHANGE COEFFICIENTS

In the bulk parameterization, the fluxes are related to the measured variables at the surface and at a certain height via the exchange coefficients. The kinematic sensible heat flux $\theta_* u_*$ and humidity flux $q_* u_*$ can be rewritten

$$\theta_* u_* = -\overline{\theta' w'} = C_H \Delta u \Delta\theta, \tag{4-122}$$

$$q_* u_* = -\overline{q' w'} = C_E \Delta u \Delta q \tag{4-123}$$

where C_H and C_E are the sensible heat and humidity exchange coefficients and Δ denotes the difference between a variable f at a certain height h and its surface value, i.e., $\Delta f = f_{z=h} - f_{z=0}$. The surface value of humidity equals its saturation value over pure water $q_0 = q_s(\theta_0)$ and $q_0 = 0.98 q_s(\theta_0)$ over saltwater (Large, Pond 1982). With q_r being the relative humidity of the air at height h, the ambient humidity at that height is $q_h = q_r q_s(\theta_h)$.

The surface boundary condition is related to the local roughness length (Makin 1998)

$$z = z^l_{0\theta}: \theta = \theta_0;\ z = z^l_{0q}: q = q_0 \tag{4-124}$$

The local roughness lengths for temperature and humidity are related to the scale of the molecular sublayer

$$z^l_{0\theta} = c_{0\theta} \frac{\nu}{u^l_*},\ z^l_{0q} = c_{0q} \frac{\nu}{u^l_*}, \tag{4-125}$$

where the proportionality coefficient $c_{0\theta}$ after Kader and Yaglom (1972) is

$$c_{0\theta} = \exp\left(-\frac{F(\mathrm{Pr})\,\kappa}{\mathrm{Pr}_t}\right), \tag{4-126}$$

and F is a function of the Prandtl number $\mathrm{Pr}=\nu/\chi_H$ ~0.70 (χ_H is the diffusivity of heat)

$$F(\mathrm{Pr}) = 12.5\,\mathrm{Pr}^{2/3} + 2.121\ln\mathrm{Pr} - 5.3. \tag{4-127}$$

From (4-125), (4-126) the value of $c_{0\theta}$ ranges from 0.18 to 0.29 in the range of the turbulent Prandtl number Pr_t from 0.9 to 1.25. Liu et al. (1979) recommend a value of $c_{0\theta}$= 0.18 for temperature and a value of c_{0q}= 0.29 for humidity. Makin and Mastenbroek (1996) showed that the solution of the model is not sensible to these constants. A value of 0.21 is adopted here for both temperature and humidity roughness lengths.

The total fluxes of heat τ_θ, equation (4-97), and humidity τ_q, equation (4-98), are constant over height. Using relations (4-99) - (4-100), equations (4-97) and (4-98) can be integrated from the surface to the top of the WBL, and the following relations can be obtained for the sensible heat and humidity exchange coefficients. For sensible heat it reads

$$C_H = C_H^0 + C_H^s, \tag{4-128}$$

where

$$C_H^0 = \left[\Delta u \int_{z_{0\theta}}^{h} K_\theta^{-1} dz\right]^{-1} \tag{4-129}$$

is the sensible heat exchange coefficient in the absence of spray (or in the presence of spray, a part which is supported by the turbulent flux τ_θ^t), and

$$C_H^s = \frac{1}{\Delta\theta}\int_{z_{0\theta}}^{h} \overset{s}{\tau}_\theta K_\theta^{-1} dz \left[\Delta u \int_{z_{0\theta}}^{h} K_\theta^{-1} dz\right]^{-1} \tag{4-130}$$

is the spray mediated exchange coefficient.

For humidity the equation is

$$C_E = C_E^0 + C_E^s, \tag{4-131}$$

where

$$C_E^0 = \left[\Delta u \int_{z_{0q}}^{h} K_q^{-1} dz\right]^{-1} \tag{4-132}$$

is the humidity exchange coefficient in the absence of spray (or in the presence of spray, a part which is supported by the turbulent flux τ_q^t), and

$$C_E^s = \frac{1}{\Delta q}\int_{z_{0q}}^{h} \overset{s}{\tau}_q K_q^{-1} dz \left[\Delta u \int_{z_{0q}}^{h} K_q^{-1} dz\right]^{-1} \tag{4-133}$$

is the spray mediated exchange coefficient.

As the evaporation function E_v is positively defined by (4-114), i.e., $E_v(z) > 0$, and thus from equation (4-92), $E(z) < 0$, the spray mediated flux of humidity, equation (4-95), is negative $\tau_q^s < 0$ while that of heat, equation ([REF:ev6]), is positive $\tau_\theta^s > 0$.

It follows from (4-128)-(4-133) that for unstable conditions ($\Delta\theta < 0$ and $\Delta q < 0$) the spray mediated coefficient $C_H^s < 0$, while $C_E^s > 0$, and thus

$$C_H < C_H^0 \tag{4-134}$$
$$C_E > C_E^0.$$

For stable conditions ($\Delta\theta > 0$ and $\Delta q > 0$) the opposite is true. The spray mediated coefficient $C_H^s > 0$ while $C_E^s < 0$, and thus

$$C_H > C_H^0 \tag{4-135}$$
$$C_E < C_E^0.$$

For the small positive value of $\Delta\theta \sim 1^\circ$ -3°, the difference $\Delta q = q_r\, q_s(\theta_s) - q_s(\theta_0)$ can be negative, depending on the value of the relative humidity q_r. In this case

$$C_H > C_H^0 \tag{4-136}$$
$$C_E > C_E^0.$$

An important conclusion can be drawn from the above analysis. If the spray mediated fluxes play a role in the balance of sensible heat and moisture over the sea, the simultaneously measured fluxes of sensible heat and humidity should show a tendency to decrease the sensible heat exchange coefficients while a tendency to increase the humidity exchange coefficients with increasing wind speed in unstable conditions, compared to their values under light and moderate winds, when spray is believed to play no role in exchanges. The situation is different for stable conditions over the sea. The sensible heat exchange coefficients have to show a tendency to increase while the humidity exchange coefficients have to show a tendency to decrease, if both $\Delta\theta$ and Δq are positive, equation (4-135). If Δq is negative, both coefficients C_H and C_E have a tendency to increase, equation (4-136).

The sensible heat and humidity exchange coefficients for unstable conditions are shown in Figure 4.14. Data of Large and Pond (1982), and Anderson (1993) of the sensible heat exchange coefficient are compiled in the same figure. Unfortunately, the

scatter of the data is so large that the model run with no spray effect (which shows a slight increase of C_H with an increase of the wind speed, contrary to the case when the spray effect is accounted for and shows a decrease in C_H) also falls well in the data cloud, and one can actually not decide which wind speed dependence of C_H is true. Data of Large and Pond (1982) for the highest wind measurement seem to offer a possibility in decreasing C_H with wind speed, which will then support a point of view that evaporation of droplets plays a role in the heat balance above the waves. However, the authors themselves approximate their data by a constant value of C_H and are not very confident in data for the highest wind, as it was a storm event. Any further speculation on comparison model results and data is dangerous before direct measurements of heat fluxes up to about 25 m s^{-1} become available, which should then reveal whether or not the impact of sea spray is important for the balance of heat and moisture.

What we can well say is that model results for wind speeds below 18 m s^{-1} support the HEXMAX conclusion that there is no drastic impact of spray on heat and humidity fluxes in this range of wind speed. We also notice that the mean value of the modeled heat exchange coefficient $10^3 C_H$ =1.1 (in the same wind speed range) agrees well with the mean estimate of Anderson (1993) of $10^3 C_H$ = 1.1 (no standard error is reported); Large and Pond (1982) of $10^3 C_H$ = 1.13±0.32 ; and HEXMAX (DeCosmo et al. 1996) of $10^3 C_H$ =1.14 ±0.35.

The calculated values of the humidity exchange coefficient are the same as the values of the heat exchange coefficient when no spray is present. However, in the presence of spray, it increases faster with wind speed, contrary to decrease in the sensible heat flux. The increase is about 20% compared to the value of C_E at a wind speed of 10 m s^{-1}. This model result seems to support a result of the HEXMAX experiment that an increase of C_E by as much as 20% is not ruled out, but a sudden and drastic increase of C_E due to evaporation of spray droplets at wind speeds beyond about 15 m s^{-1} is not found (measurements were made up to 18 m s^{-1} in unstable conditions). Again, that remark remains pure speculation unless reliable data at wind speeds of about 25 m s^{-1} become available.

Results of modeling the exchange coefficients in stable conditions Figure 4.15 give the same conclusions. The mean value of calculated sensible heat exchange coefficient $10^3 C_H$ = 0.78 agrees well with measurement: Large and Pond (1982) give $10^3 C_H$ = 0.66 ±0.14 ; Anderson (1993) gives $10^3 C_H$ = 0.79. The impact of evaporating droplets is not noticeable below 18 m s^{-1}. Notice that while in strong stable conditions the impact of spray will lead to an increase of the heat exchange coefficient and decrease of the humidity exchange coefficient, both will increase in weak stable conditions. These trends (if they exist) should be measurable at wind speeds of about 25 m s^{-1}.

Direct measurements of sensible heat and humidity flux at wind speeds of about 25 m s^{-1} should give a clear answer as to whether the sea spray plays an important role in exchanges of heat and humidity or not.

It is important to note, that in the absence of spray mediated fluxes the model show only a marginal wind speed dependence of the sensible heat and humidity exchange coefficients, contrary to the strong wind speed dependence of the drag coefficient. The different wind speed dependence of the drag coefficient and sensible heat exchange coefficient can be explained by the difference in exchange mechanism of momentum and heat at the sea surface (Makin, Mastenbroek 1996). Momentum to a large extend is transported by the organised wave-induced motions correlated with the waves (the form drag, equation (4-7). Heat and moisture are transported only by viscosity, equations (4-

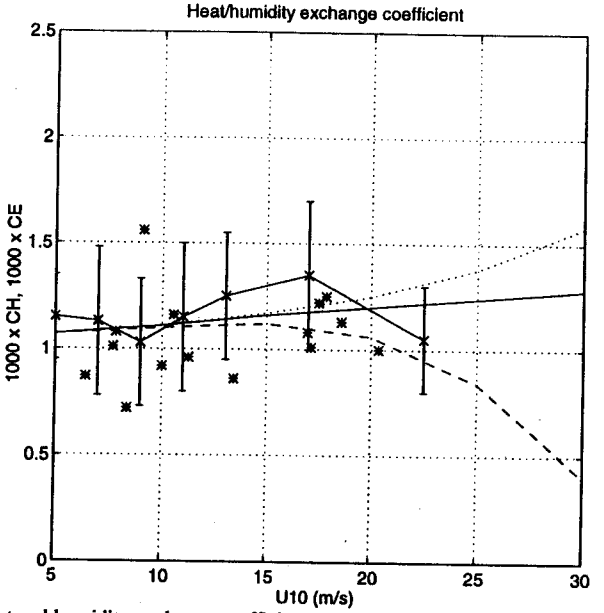

Figure 4.14 Heat and humidity exchange coefficient versus U_{10}, unstable stratification ($\Delta\theta = -3°$). For the heat exchange coefficient, stars show data of Anderson (1993), unstable conditions, compiled from his Figure 8a. Solid line with crosses and error bars are data of Large and Pond (1982, Figure 10). Model results are shown as follows: solid line, no spray effect; dashed line, spray effect is accounted for. For the humidity exchange coefficient, model results are shown as follows: solid line, no spray effect; dotted line, spray effect is accounted for.

97)-(4-98) with $\tau'_\theta = \tau'_q = 0$. The form drag dominates the surface stress and determines the vertical structure of turbulence in the WBL. The sensible heat and humidity flux above waves is determined by the diffusivity of turbulence, equation ([REF:k]), which is affected by waves. In this case waves have only indirect impact on heat and humidity fluxes. It is well established by field measurements that the sensible heat and humidity exchange coefficients over the sea are much less dependent on the wind speed in the range of measurements (< 20 m/s) than the drag coefficient (Anderson 1993; DeCosmo et al. 1996; Friehe, Schmitt 1976; Geernaert 1990; Katsaros et al. 1987, 1994; Large, Pond 1982; Smith 1980, 1988, 1989). For practical applications the sensible heat and humidity exchange coefficients are taken usually as constants, i.e. wind speed independent (Anderson 1993; DeCosmo et al. 1996; Friehe, Schmitt, 1976; Large, Pond 1982; Smith 1980, 1988, 1989).

4.8 Discussion

A theory of dynamical coupling surface waves with the atmosphere, which allows consistent description of momentum and heat exchange processes at the sea surface in presence of waves and sea spray, is presented here. The approach is based on conservation of momentum and heat in the marine atmospheric surface boundary layer. The total stress is supported by turbulent stress and by the wave-induced stress due to

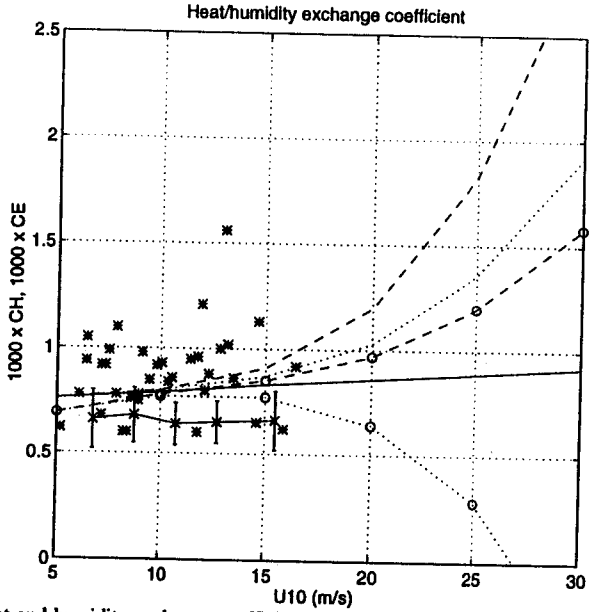

Figure 4.15 Heat and humidity exchange coefficient versus U_{10}, stable stratification ($\Delta\theta = +1.5^{\circ}$). For the heat exchange coefficient, stars show data of Anderson (1993), stable conditions, compiled from his Figure 8a. Solid line with crosses and error bars are data of Large and Pond (1982, Figure 10). Model results are shown as follows: solid line, no spray effect; dashed line, spray effect is accounted for ($\Delta\theta = +1.5^{\circ}$); dashed line with circles, $\Delta\theta = +5^{\circ}$. For the humidity exchange coefficient, model results are shown as follows: solid line, no spray effect; dotted line, spray effect is accounted for ($\Delta\theta = +1.5^{\circ}$); dotted line with circles, $\Delta\theta = +5^{\circ}$.

the presence of waves. The total heat flux is supported by turbulent flux, and by spray mediated flux resulting from evaporation of droplets produced by wave breaking. The basic idea concerns the properties of viscous momentum and heat exchange at the sea surface, and postulates that at the surface momentum and heat are transported by molecular diffusivity inside the viscous sublayer covering the instantaneous water surface. This idea allows to avoid the parameterization of the background roughness parameter in terms of the Charnock-type relation, a serious drawback of the first wind over waves coupling theories by Janssen (1989), and by Chalikov and Makin (1991). In the frame of presented theory, the description of the surface boundary layer results from a self-consistency between waves (described by the wave spectrum), momentum and energy input to waves from the wind, and a balance between the turbulent and wave-induced fluxes. The model of wind over waves coupling is viewed as a high order parameterization of the marine atmospheric surface boundary layer, compared to the standard bulk parameterization.

Short wind waves (wave length is from few millimetres to few decimeters) play an important role in the air-sea interaction as they are strongly coupled to the atmosphere and support a significant part of stress at the surface. A physical model of short waves by Kudryavtsev (1996) and by Kudryavtsev et al. (1997) is used here to dynamically couple waves with the atmosphere. It this model, the form of the wave spectrum results from a balance in the energy spectral density from wind input, nonlinear wave-wave

interactions, dissipation due to wave breaking and viscous dissipation, and cascade nonlinear interactions responsible for generation of parasitic capillaries by short gravity waves. The model of the wave spectrum quantitatively reproduce the known empirical statistical properties of the sea surface, in particular the shape of the short wave spectrum, dependence of its spectral level on wind speed, angular spreading of energy, mean square slope of the sea surface.

Ensuring the correct description of the sea state in terms of a wave spectrum, it is shown that for moderate and high wind speeds most of the surface stress is supported by waves. For lower wind speeds, a considerable part of the stress is supported by viscous drag. For light winds this permits experimentally observed aerodynamically smooth or transitional conditions of the sea surface. The form drag, the part of the surface stress supported by waves, is shown to be formed by waves shorter than 10 m, and more than 50% of it is supported by waves shorter than 1 m. It appears that the form of the wave spectrum in the high wave number range to a large extent determines the sea drag.

The problem of the wave age dependence of the sea drag is readdressed to the wave age dependence of the high wave number tail of the wave spectra. We argue that the sea drag will depend on the wave age only if the tail of the wave spectra feels this dependence. We are not aware of direct experimental evidence that short waves depend on wave age. We are not aware as well on convincing direct measurements of the sea drag, made at the same site, which will show this dependence. To gain further insight in this complicated problem, simultaneous measurements of the stress and the directional wave number spectrum in the full wave number range are highly desirable.

For wind speeds lower than 18 m/s the impact of the sea spray on heat fluxes does not show up in the field measurements. In this regime, the different wind speed dependence of the drag coefficient (almost linear increase with the wind speed) and heat exchange coefficients (marginal or no increase with the wind speed) is explained by the fact, that while momentum to a large extend is transported by the organized wave-induced motions correlated with the waves (by the form drag), heat is transported by viscosity alone.

Relating concentration of sea droplets, produced by wave breaking, to the whitecap coverage of the sea surface, and their vertical decay length to the significant wave height we calculate the sensible heat and humidity fluxes directly from the wind speed and the sea state. Satisfying the experimental fact that in the range of wind speed < 18 m/s no impact of sea spray on heat and humidity fluxes is detected we show that the impact of spray becomes significant at wind speeds of about 25 m/s and above.

The proposed coupled model of the sea surface-atmosphere can be potentially used in air-sea interaction studies, in coupling atmosphere circulation models to the ocean via the surface waves, and in electromagnetic models of the sea surface.

4.9 References

Anderson, R.J. (1993) 'A study of wind stress and heat flux over the open ocean by the inertial-dissipation method', *J. Phys.Oceanogr.*, **23**, 2153-2161.

Andreas, E.L. (1992) Sea spray and the turbulent air- sea heat fluxes, *J. Geophys. Res.*, *97*, 11,429- 11,441, 1992.

Andreas, E.L. (1994) 'Reply', *J. Geophys. Res.*, *99*, 14,345-14,350.

Andreas, E.L., Edson, J.B., Monahan, E.C., Rouault, M.P., Smith, S.D. (1995) The spray contribution to net evaporation from the sea: a review of recent progress, *Boundary Layer Meteorol.*, *72*, 3-52.

Apel, J.R. (1994) An improved model of the ocean surface wave vector spectrum and its effects on radar backscatter, *J. Geophys. Res.*, **99**, 16.269 - 16.290.

Banner, M.L., Jones, I.S.F., Trinder, J.C. (1989) Wavenumber spectra of short gravity waves, *J.Fluid Mech.*, **198**, 321-344.

Banner, M.L., Peirson, W.L. (1996) Tangential stress beneath wind-driven air-water interface, *AMR 96/19, University of New South Wales, March 1996*, submitted to *J.Fluid Mech.*.

Belcher, S.E., Hunt, J.C.R. (1993) 'Turbulent shear flow over slowly moving waves,' *J. Fluid Mech.*, **251**, 109-148.

Caudal, G. (1993) 'Self-consistency between wind stress, wave spectrum, and wind-induced wave growth for fully rough air-sea interface', *J. Geophys. Res.*, **98**, C12, 22743-22752.

Chalikov, D.V., Makin, V.K. (1991) 'Models of the wave boundary layer', *Boundary-Layer Meteorol.*, **56**, 83-99.

Chalikov, D.V., Belevich, M. Yu. (1993) One- dimensional theory of the wave boundary layer', *Boundary-Layer Meteorol.*, **63**, 65-96.

Chang, J.H., Wagner, R.N., Henry, C.Y. (1978) Measurements of high frequency capillary waves on steep gravity waves. *J.Fluid Mech.*, **83**, 401-415.

Charnock, H. (1955) 'Wind stress on a water surface', *Quart.J.Roy. Meteorol. Soc.*, **81**, 639- 640.

Cox, C.S. (1958) Measurements of slopes of high frequency waves, *J. Mar. Res.*, **16**, 199-225.

Cox, C.S., Munk, W.H. (1954) 'Statistics of the sea derived from sun glitter', *J. Mar. res.*, **13**, 198-227.

Crapper, G.D. (1970) Non-linear capillary waves generated by steep gravity waves, *J.Fluid Mech.*, **40**, 149-159.

DeCosmo, J., Katsaros, K.B., Smith, S.D., Anderson, R.J., Oost, W.A., Bumke, K., Chadwick, H. (1996) Air-sea exchange of water vapor and sensible heat: The Humidity Exchange Over the Sea (HEXOS) results, *J. Geophys. Res.*, *101*, 12,001-12,016.

Donelan, M.A. (1990) Air-sea interaction, in *The Sea: Ocean Engineering Science*, **9**, 239-292.

Donelan, M.A., Pierson, W.J. (1987) 'Radar scattering and equilibrium ranges in wind-generated waves with application to scatterometry', *J. Geophys. Res.*, **92**,(C5), 4971-5029.

Donelan, M.A., Hamilton, J., Hui, W.H. (1985) Directional spectra of wind generated waves, *Phil. Trans. Royal Soc. London*, Ser.A, **315**, 509-562.

Donelan, M.A., Dobson, F.W., Smith, S.D., Anderson, R.J. (1993) 'On the dependence of sea-surface roughness on wave development', *J. Phys. Oceanogr.*, **23**, 2143-2149.

Donelan, M.A., Dobson, F.W., Smith, S.D., Anderson, R.J. (1995) 'Reply', *J. Phys. Oceanogr.*, **25**, 1908-1909.

Duncan, J.H. (1981) An experimental investigation of breaking waves produced by towed hydrofoil, *Proc. R. Soc. London*, **A377**, 331-348.

Dyer, A.J. (1974) 'A review of flux-profile relationships', *Boundary-Layer Meteor.*, **7**, 363- 372.

Edson, J.B., Fairall, C.W. (1994) Spray droplet modeling, 1, Lagrangian model simulation of the turbulent transport of evaporating droplets, *J. Geophys. Res.*, *99*, 25,295-25,311.

Edson, J.B., Anquetin, S., Mestayer, P.G., Sini, J.F. (1996) Spray droplet modeling, 2, An interactive Eulerian- Lagrangian model of evaporating spray droplets, *J. Geophys. Res.*, *101*, 1279-1293.

Elfouhaily, T., Chapron, B., Katsaros, K., Vandemark, D. (1997) A Unified directional spectrum for long and short wind-driven waves, *J. Geophys. Res*, **107**, 15781-15796.

Fairall, C.W., Kepert, J.D., Holland, G.J. (1994) The effect of sea spray on surface energy transports over the ocean, *Global Atmos. Ocean Syst.*, 2, 121-142.

Friehe, C.A., Schmitt, K.F. (1976) Parameterizations of air-sea interface fluxes of sensible heat and moisture by the bulk aerodynamic formulas, *J. Phys. Oceanogr.*, *6*, 801-809.

Geernaert, G.L. (1990) Bulk parameterizations for the wind stress and heat fluxes, in *Surface Waves and Fluxes, vol.1*, edited by G.L. Geernaert and W.J. Plant, 336 pp., Kluwer Acad., Norwell, Mass.

Gent, P.R., Taylor, P.A.(1976) 'A numerical model of the air-flow over waves', *J. Fluid Mech.*, **77**, 105-128.

Hara, T., Bock, E.J., Donelan, M. (1997) 'Frequency-wavenumber spectrum of wind-generated gravity-capillary waves', *J. Geophys. Res.*, **102**, 1067-1072.

Harris, J.A., Belcher, S.E., Street, R.L. (1996) 'Linear dynamics of wind waves in coupled turbulent air- water flow. Part 2. Numerical model.', *J. Fluid Mech.*, **308**, 219-254.

Hasse, L. (1992) On the contribution of spray droplets to evaporation, *Boundary Layer Meteorol.*, *61*, 309- 313.

Hasselmann, K. (1968) 'Weak-interaction theory of ocean waves', *Basic Developments in Fluid Dynamics*, **2**, 117-182.

Hasselmann, K. (1962) 'On the non-linear energy transfer in a gravity wave spectrum. Part 1.', *J. Fluid Mech.*, **12**, 481-500.

Hunt, J.C.R., Cohen, J.E., Belcher, S:E., Wood, N. (1997) 'Turbulent flow over growing waves', *Proceedings of the IMA Conference on Wind-Over Waves Coupling: Perspective and Prospects*, 8th-10th April 1997, University of Salford, UK.

Hwang, P.A. (1996) 'Short ocean waves and air- sea interaction', *The preprint volume of the Eighth Conference on Air-Sea Interaction and Symposium on GOALS*, 28 January - 2 February 1996, Atlanta, GA by the American Meteorological Society, Boston, MA.

Hwang, P.A., Atakturk, S., Sletten, M.A., Trizna, D.B.(1996) 'A study of the wavenumber spectra of short water waves in the ocean', *J. Phys. Oceanogr.*, **26**, 1266-1285.

Jähne, B., Riemer, K.S. (1990) 'Two- dimensional wave number spectra of small-scale water surface waves' *J. Geophys. Res.*, **95**, 11531-11546.

Janssen, J.A.M. (1997) 'Does wind stress depend on sea-state or not? -A statistical error analysis of HEXMAX data', *Boundary-Layer Meteorol.*, **83**, 479-503.

Janssen, P.A.E.M. (1989) 'Wave-Induced Stress and the Drag of Air Flow over Sea Waves', *J. Phys.Oceanogr.*, **19**, 745-754.

Janssen, P.A.E.M. (1994) Results with a coupled wind wave model, *ECMWF Res. Dept. Techn. Report*, **71**, ECMWF, Reading, 58p.

Janssen, P.A.E.M., Viterbo, P. (1995) 'Ocean waves and atmospheric climate', *J. of Climate*, **9**, 1269-1287.

Jenkins, A.D. (1993) A simplified quasi-linear model for wave generation and air-sea momentum flux, *J. Phys. Oceanogr.*, *23*, 2001-2018.

Jones, I.S.F., Toba, Y. (1995) 'Comments on "The dependence of sea-surface roughness on wave development"', *J. Phys. Oceanogr.*, **25**, 1905-1907.

Kader, B.A., Yaglom, A.M. (1972) Heat and mass transfer laws for fully turbulent wall flows, *Int. J. Heat Mass Transfer*, *15*, 2329-2353, 1972.

Katsaros, K.B., Smith, S.D., Oost, W.A. (1987) HEXOS - Humidity Exchange Over the Sea: A program for research on water vapor and droplet fluxes from sea to air at moderate and high wind speeds, *Bull. Am. Meteorol. Soc.*, *68*, 466-476.

Katsaros, K.B., DeCosmo, J., Anderson, R.J., Smith, S.D., Kraan, C., Oost, W.A., Hasse, L., Bumke, K., Mestayer, P.G., Smith M.H. (1994) Measurements of humidity and temperature in the marine environment during the HEXOS Main Experiment, *J. Atmos. Ocean. Technol.*, *11*, 964-981.

Kitaigorodskii, S.A. (1983) On the theory of the equilibrium range in the spectrum of wind-generated gravity waves, *J. Phys. Oceanogr.*, **13**, 816-827.

Klinke, J., Jähne, B. (1992). 2D wave number spectra of short wind waves - results from wind wave facilities and extrapolation to the ocean, in *Optics of the Air-Sea Interface: Theory and Measurements*, Proc. SPIE 1749, Int. Soc. Opt. Ent., 1-13.

Komen, G.J., Cavalery, L., Donelan, M., Hasselmann, K., Hasselmann, S., Janssen, P.A.E.M. (1994) *Dynamics and modelling of ocean waves*, Cambridge Univ. Press, 540 pp.

Komen, G., Janssen, P.A.E.M., Makin, V., Oost, W. (1998) 'On the sea state dependence of the Charnock parameter', *The Glob. Atmos. and Ocean Syst.*, , in press.

Kudryavtsev, V.N. (1996) 'A physical model of the capillary-gravity wave spectrum', *Marine Hydrophysical J.*, **96**, 3-14.

Kudryavtsev, V.N., Makin, V.K., Chapron, B. (1997) ' Coupled sea surface-atmosphere model. Part 2. Spectrum of short wind waves', KNMI MEMO WM-97-10, submitted to *J. Geophys. Res.*.

Large, W.G., Pond, S. (1982) 'Sensible and latent heat flux measurements over the ocean', *J. Phys.Oceanogr.*, **12**, 464-482.

Liu, W.T., Katsaros, K.B., Businger, J.A. (1979) Bulk parameterization of air-sea exchanges of heat and water vapor including the molecular constrains at the interface, *J. Atmos. Sci.*, *36*, 1722-1735.

Longuet-Higgins M.S. (1963) 'The generation of capillary waves by steep gravity waves', *J. Fluid Mech.*, **16**, 138-159.

Longuet-Higgins, M.S. (1982) On the skewness of sea-surface slopes, *J. Phys. Oceanogr.*, **12**, 1283-1291.

Makin, V.K. (1989) 'The dynamics and structure of the boundary layer above sea', Senior doctorate thesis, Inst. of Oceanology, Acad. of Sci. USSR, Moscow, 417 pp.

Makin, V.K. (1990) 'Deviation of the mean wind profile above waves from the logarithmic distribution', *Izv. Atm. Ocean Phys.*, **26**, 322-324.

Makin, V.K. (1997) 'Coupling of waves with the atmosphere', *Proceedings of the IMA Conference on Wind-Over Waves Coupling: Perspective and Prospects*, 8th-10th April 1997, University of Salford, UK.

Makin, V.K. (1998) 'Air-sea exchange of heat in the presence of wind waves and spray', *J. Geophys. Res.*, **103**, 1137-1152.

Makin, V.K., Kudryavtsev, V.N. (1997) Coupled sea surface-atmosphere model. Part 1. Wind over waves coupling, KNMI MEMO WM-97-11, submitted to *J. Geophys. Res.*.

Makin, V.K., Mastenbroek, C. (1996) 'Impact of waves on air-sea exchange of sensible heat and momentum', *Boundary-Layer Meteor.*, **79**, 279-300.

Makin, V.K., Kudryavtsev, V.N., Mastenbroek, C. (1995) 'Drag of the sea surface', *Boundary-Layer Meteorol.*, **73**, 159-182.

Mastenbroek, C. (1996) *Wind-Wave Interaction*, PhD Thesis, University of Delft, 119 pp.
Mastenbroek, C., Burgers, G.J.H., Janssen, P.A.E.M. (1993) 'The dynamical coupling of a wave model and a storm surge model through the atmospheric boundary layer', *J. Phys. Oceanogr.*, **23**, 1856-1866.
Mastenbroek, C., Makin, V.K., Garat, M.H., Giovanangeli, J.P. (1996) 'Experimental evidence of the rapid distortion of turbulence in the air flow over water waves', *J. Fluid Mech.*, **318**, 273-302.
Monahan, E.C., Spiel, D.E., Davidson, K.L. (1986) 'A model of marine aerosol generation via whitecaps and wave disruption', in *Oceanic Whitecaps and Their Role in Air-Sea Exchange Processes* , edited by E.C. Monahan and G. Mac Niocaill, 167-174, D. Reidel, Dordrecht.
Monin, A.S., Yaglom, A.M. (1971) *Statistical Fluid Mechanics*, Vol. 1, Cambridge: MIT Press, 769 pp.
Miles, J.W. (1957) 'On the generation of surface waves by shear flows', *J. Fluid Mech.*, **3**, 185-204.
Oost, W.A. (1998) 'The KNMI HEXMAX stress data - a revisit', *Boundary-Layer Meteorol.*, , in press.
Phillips, O.M. (1966) *The Dynamics of the Upper Ocean*, 1st ed. Cambridge University Press, 261 pp.
Phillips, O.M. (1985) Spectral and statistical properties of the equilibrium range in the wind-generated gravity waves, *J. Fluid Mech.*, **156**, 505-531.
Plant, W.J. (1982) 'A relation between wind stress and wave slope', *J. Geophys. Res.*, **87**, 1961-1967.
Preobrazhenskii, L.Y. (1973) Estimate of the content of spray-drops in the near-water layer of the atmosphere, *Fluid Mech. Sov. Res.*, **2**, 95-100.
Pruppacher, H.R., Klett, J.D. (1978) *Microphysics of Clouds and Precipitation*, 714 pp., D. Reidel, Norwell, Mass.
Rodi, W. (1984) *Turbulence Models and Their Application in Hydraulics - A State of the Art Review*, 2nd ed., 104 pp., Inst. fur Hydromech. Univ. of Karlsruhe, Int. Assoc. for Hydraul. Res., Karlsruhe.
Ruvinsky, K.D., Feldstein, F.I., Freidman, G.I. (1991) Numerical simulation of the quasi-stationary stage of ripple excitation by steep gravity-capillary waves, *J. Fluid Mech.*, **230**, 339-353.
Smith, M.H., Park, P.M., Consterdine, I.E. (1993) Marine aerosol concentrations and estimated fluxes over the sea, *Q. J. R. Meteorol. Soc.*, *119*, 809-824.
Smith, S.D. (1980) Wind stress and heat flux over the ocean in gale force winds, *J. Phys. Oceanogr.*, *10*, 709-726.
Smith, S.D. (1988) Coefficients for sea surface wind stress, heat flux and wind profiles as a function of wind speed and temperature, *J. Geophys. Res.*, *93*, 15,467-15,472.
Smith, S.D. (1989) Water vapour flux at the sea surface, *Boundary Layer Meteorol.*, *47*, 277-283.
Smith, S.D., Katsaros, K.B., Oost, W.A., Mestayer, P.G. (1996) The impact of the HEXOS programme, *Boundary Layer Meteorol.*, *78*, 121-141.
Smith, S.D., Anderson, R.J., Oost, W.A., Kraan, C., Maat, N., DeCosmo, J., Katsaros, K.B., Davidson, K.L., Bumke, K., Hasse, L. Chadwick, H.M. (1992) 'Sea surface wind stress and drag coefficients: the HEXOS results', *Boundary-Layer Meteorol.*, **60**, 109-142.
Snyder, R.L., Dobson, F.W., Elliott J.A., Long, R.B. (1981) 'Array measurements of atmospheric pressure fluctuations above surface gravity waves', *J. Fluid Mech.*, **102**, 1-59.
Stull, R.B. (1991) *An Introduction to Boundary Layer Meteorology*, 666 pp., Kluwer Acad., Norwell, Mass..
Toba, Y. (1973) Local balance in the air-sea boundary processes. III. On the spectrum of wind waves, *J. Ocean Soc. Japan*, **29**, 209-220.
Toba, Y., Iida, N., Kawamura, N., Jones, I.S.F. (1990) 'The wave dependence of sea-surface wind stress', *J. Phys. Oceanogr.*, **20**, 705-721.
Townsend, A.A. (1956) *The Structure of Turbulent Shear Flow*, Cambridge University Press.
Valenzuela, G.R., Laing, M.B. (1972) 'Nonlinear energy transfer in gravity-capillary wave spectra, with applications', *J. Fluid Mech.*, **54**, 507-520.
Wu, J. (1988) Bubbles in the near-surface ocean: A general description, *J. Geophys. Res.*, *93*, 587- 590.
Wu, J. (1989) Contributions of film and jet droplets to marine aerosols produced at the sea surface, *Tellus*, *41B*, 469-473.
Wu, J. (1990) 'Mean square slopes of the wind- disturbed water surface, their magnitude, directionality and composition', *Radio Science*, **25**, 37-48.
Wu, J. (1990) On parameterization of sea spray, *J. Geophys. Res.*, *95*, 18,269-18,279.
Wu, J. (1992) Bubble flux and marine aerosol spectra under various wind velocities, *J. Geophys. Res.*, *97*, 2327-2333.
Yelland, M., Taylor, P.K.(1996) 'Wind stress measurements from the open ocean', *J. Phys. Oceanogr.*, **26**, 541-558.
Yermakov, S.A., Ruvinskiy, K.D., Salashin, S.G., Freydman, G.I. (1986) Experimental investigation of the generation of capillary-gravity ripples by strongly non-linear waves on the surface of a deep fluid, *Izv. Atmos. Ocean Phys.*, **22**, 835-842.
Zhang, X. (1995) Capillary-gravity and capillary waves generated in a wind wave tank: observations and theories, *J. Fluid Mech.*, **289**, 51-82.
Zakharov, V.Ye., Zaslavskii, M.M. (1982) The kinetic equation and Kolmogorov spectra in a low turbulence theory of wind waves, *Izv. Atmos. Ocean Phys.*, **18**, 747-753.
Zilitinkevich, S.S. (1970) *The Dynamics of the Atmospheric Boundary Layer*, 292 pp., Gidrometeoizdat, Leningrad.